THE EUROPEAN
PHYSICAL JOURNAL C

CrossMark

Heavy Higgs decays into sfermions in the complex MSSM: a full one-loop analysis

S. Heinemeyer[1,a], **C. Schappacher**[2,b]

[1] Instituto de Física de Cantabria (CSIC-UC), Santander, Spain
[2] Institut für Theoretische Physik, Karlsruhe Institute of Technology, 76128 Karlsruhe, Germany

Abstract For the search for additional Higgs bosons in the Minimal Supersymmetric Standard Model (MSSM) as well as for future precision analyses in the Higgs sector a precise knowledge of their decay properties is mandatory. We evaluate all two-body decay modes of the heavy Higgs bosons into sfermions in the MSSM with complex parameters (cMSSM). The evaluation is based on a full one-loop calculation of all decay channels, also including hard QED and QCD radiation. The dependence of the heavy Higgs bosons on the relevant cMSSM parameters is analyzed numerically. We find sizable contributions to many partial decay widths. They are roughly of $\mathcal{O}(15\,\%)$ of the tree-level results, but can go up to 30 % or higher. The size of the electroweak one-loop corrections can be as large as the QCD corrections. The full one-loop contributions are important for the correct interpretation of heavy Higgs-boson search results at the LHC and, if kinematically allowed, at a future linear e^+e^- collider. The evaluation of the branching ratios of the heavy Higgs bosons will be implemented into the Fortran code `FeynHiggs`.

1 Introduction

One of the most important tasks at the LHC is to search for physics effects beyond the Standard Model (SM), where the Minimal Supersymmetric Standard Model (MSSM) [1–4] is one of the leading candidates. Supersymmetry (SUSY) predicts two scalar partners for all SM fermions as well as fermionic partners to all SM bosons. Another important task is investigating the mechanism of electroweak symmetry breaking. The most frequently investigated models are the Higgs mechanism within the SM and within the MSSM.

C. Schappacher was formerly affiliated with Institut für Theoretische Physik, Karlsruhe Institute of Technology.

[a] e-mail: Sven.Heinemeyer@cern.ch
[b] e-mail: schappacher@kabelbw.de

Contrary to the case of the SM, in the MSSM two Higgs doublets are required. This results in five physical Higgs bosons instead of the single Higgs boson in the SM; three neutral Higgs bosons, h_n ($n = 1, 2, 3$), and two charged Higgs bosons, $H^\pm$. The Higgs sector is described at the tree level by two parameters: the mass of the charged Higgs boson, $M_{H^\pm}$, and the ratio of the two vacuum expectation values, $\tan\beta \equiv t_\beta = v_2/v_1$. Often the lightest Higgs boson, h_1 is identified with the particle discovered at the LHC [5,6] with a mass around ∼125 GeV. If the mass of the charged Higgs boson is assumed to be larger than ∼200 GeV the four additional Higgs bosons are roughly mass degenerate, $M_{H^\pm} \approx m_{h_2} \approx m_{h_3}$, and they are referred to as the "heavy Higgs bosons". Discovering one or more of those additional Higgs bosons would be an unambiguous sign of physics beyond the SM and could yield important information as regards their supersymmetric origin.

If SUSY is realized in nature and the charged Higgs-boson mass is $M_{H^\pm} \lesssim 1.5$ TeV, then the heavy Higgs bosons could be detectable at the LHC [7,8] (including its high luminosity upgrade, HL-LHC; see Ref. [9] and references therein) and/or at a future linear e^+e^- collider such as the ILC [10–14] or CLIC [15,16]. (Results on the combination of LHC and LC results can be found in Refs. [17–19].) The discovery potential at the HL-LHC goes up to $\mathcal{O}(1\text{ TeV})$ for large $\tan\beta$ values and somewhat lower at low $\tan\beta$ values. At an e^+e^- linear collider the heavy Higgs bosons are pair produced, and the reach is limited by the center-of-mass energy, $M_{H^\pm} \lesssim \sqrt{s}/2$, roughly independent of $\tan\beta$. Details as regards the discovery process(es) depend strongly on the cMSSM parameters (and will not be further discussed in this paper).

In the case of a discovery of additional Higgs bosons a subsequent precision determination of their properties will be crucial to determine their nature and the underlying (SUSY) parameters. In order to yield a sufficient accuracy, one-loop corrections to the various Higgs-boson decay modes have to be considered. Decays to SM fermions have been evaluated

Springer

at the full one-loop level in the cMSSM in Ref. [20]; see also Refs. [21] as well as Refs. [22–28] for higher-order SUSY corrections. Decays to (lighter) Higgs bosons have been evaluated at the full one-loop level in the cMSSM in Ref. [20]; see also Ref. [29]. Decays to SM gauge bosons can be evaluated to a very high precision using the full SM one-loop result [30–32] combined with the appropriate effective couplings [33]. The full one-loop corrections in the cMSSM listed here together with resummed SUSY corrections have been implemented into the code FeynHiggs [33–38]. Corrections at and beyond the one-loop level in the MSSM with real parameters (rMSSM) are implemented into the code HDECAY [39–41]. Both codes were combined by the LHC Higgs Cross Section Working Group to obtain the most precise evaluation for rMSSM Higgs-boson decays to SM particles and decays to lighter Higgs bosons [42].

The heavy MSSM Higgs bosons can also decay to SUSY particles, i.e. to charginos, neutralinos, and scalar fermions. In Ref. [43] it was demonstrated that the SUSY particle modes can dominate the decay of the heavy Higgs bosons. In this work we calculate all two-body decay modes of the heavy Higgs bosons to scalar fermions in the cMSSM.[1] More specifically, we calculate the full one-loop corrections to the partial decay widths

$$\Gamma(h_n \to \tilde{f}_i \tilde{f}_j^\dagger) \quad (n = 2, 3;\ i, j = 1, 2), \tag{1}$$

$$\Gamma(H^+ \to \tilde{f}_i \tilde{f}_j'^\dagger) \quad \text{and} \quad \Gamma(H^- \to \tilde{f}_i^\dagger \tilde{f}_j') \quad (i, j = 1, 2), \tag{2}$$

where $H^\pm$ denotes the charged, h_n the mixed neutral Higgs bosons and $\tilde{f}$ ($\tilde{f}^\dagger$) denotes the scalar (anti-) fermions.[2] The total decay width is defined as the sum of the partial decay widths (1) or (2), the SM decay channels as described above and the decays to charginos/neutralinos (at the tree level, supplemented with effective couplings [33]).

The evaluation of the channels Eqs. (1), (2) is based on a full one-loop calculation, i.e. including (S)QCD and electroweak (EW) corrections, as well as soft and hard QCD and QED radiation. For "mixed" decay modes, we evaluate in addition the two "$\mathcal{CP}$-versions" ($i \neq j$) of Eq. (1) and the two "$\mathcal{CP}$-versions" of Eq. (2), which give different results for non-zero complex phases. While our calculation comprises the decay to *all* sfermionic decay modes of the cMSSM Higgs bosons, in our numerical analysis we will focus on the decay to the third generation sfermions, scalar top and bottom quarks, scalar tau and tau neutrinos.

Higher-order contributions to MSSM Higgs decays to scalar fermions have been evaluated in various analyses over the last decade. However, they were in most cases restricted

to a few specific channels. In many cases only parts of a one-loop calculation has been performed, and no higher-order corrections in the cMSSM are available so far. More specifically, the available literature comprises the following. First, $\mathcal{O}(\alpha_s)$ corrections to partial decay widths of various squark decay channels in the rMSSM were derived: to the decay of a charged Higgs to stops and sbottoms in Ref. [44], of a heavy Higgs boson to third generation squarks in Ref. [45], supplemented later by an effective resummation of the trilinear Higgs-sbottom coupling in Ref. [46]. First full one-loop corrections in the rMSSM were calculated in the decays of the $\mathcal{CP}$-odd Higgs boson to scalar quarks [47] and to scalar fermions [48]. The full one-loop corrections in the rMSSM to Higgs decays to squarks was published in Ref. [49]. More recently, the results of this group were made public in the code HFOLD [50], using a pure $\overline{\text{DR}}$ renormalization for the calculation. While their results constitute a full one-loop correction (although not for complex parameters), it differs from our calculation in the renormalization of the SUSY particles and parameters. It was shown in Refs. [51–54] that our renormalization leads to stable results over nearly the full cMSSM parameters space.

The full $\mathcal{O}(\alpha_s)$ corrections to Higgs decays to scalar quarks were also evaluated by a different group in Ref. [55], using a renormalization more similar to ours, but also restricting to the case of real parameters. Finally, in Ref. [56] the $\mathcal{O}(\alpha_s)$ corrections to Higgs decays to scalar quarks were re-analyzed, where the emphasis was put on the connection of the MSSM squark sector and Higgs sector couplings to $\overline{\text{MS}}$ input parameters. The latter corrections in particular differ from our treatment of the renormalization of the scalar quark sector. They have been included into the code HDECAY.

In this paper we present for the first time a full one-loop calculation for all two-body sfermionic decay channels of the Higgs bosons in the cMSSM (with no generation mixing), taking into account soft and hard QED and QCD radiation. In Sect. 2 we review the renormalization of all relevant sectors of the cMSSM. Details about the calculation can be found in Sect. 3, and the numerical results for all decay channels are presented in Sect. 4 (including comments on comparisons with results from other groups). The conclusions can be found in Sect. 5. The results will be implemented into the Fortran code FeynHiggs [33–38].

2 The complex MSSM

The channels (1) and (2) are calculated at the one-loop level, including hard QED and QCD radiation. This requires the simultaneous renormalization of several sectors of the cMSSM, including the colored sector with top and bottom quarks and their scalar partners and the Higgs and gauge-boson sector with all the Higgs bosons as well as the Z and

---

[1] We neglect flavor violation effects and resulting decay channels.

[2] In the text and figures below we omit the † (denoting anti-particles) for simplification.

the W boson and the chargino/neutralino sector. In the following subsections we briefly review these sectors and their renormalization.

2.1 The Higgs- and gauge-boson sector

The Higgs- and gauge-boson sector follow strictly Ref. [57] and references therein (see especially Ref. [33]). This defines in particular the counterterm $\delta \tan \beta \equiv \delta t_\beta$, as well as the counterterms for the Z boson mass, δM_Z^2, and the sine of the weak mixing angle, δs_w.

2.2 The chargino/neutralino sector

The chargino/neutralino sector is also described in detail in Ref. [57] and references therein. In this paper we use the so called CCN scheme, i.e. on-shell conditions for two charginos and one neutralino, which we chose to be the lightest one. In the notation of Ref. [57] we used:

$InoScheme = CCN[1] – fixed CCN scheme with on-shell $\tilde{\chi}_1^0$.

This defines in particular the counterterm $\delta \mu$, where μ denotes the Higgs mixing parameter.

2.3 The fermion sector

The fermion sector is described in detail in Ref. [57] and references therein. For simplification we use here the $\overline{\text{DR}}$ renormalization for all three generations of down-type quarks *and* leptons, again in the notation of Ref. [57]:

UVMf1[4,_] = UVDivergentPart
$\overline{\text{DR}}$renormalization for m_d, m_s, m_b

UVMf1[2,_] = UVDivergentPart
$\overline{\text{DR}}$ renormalization for m_e, m_μ, m_τ

2.4 The scalar fermion sector

The renormalization of the sfermion sector which we use here differs slightly from the one described in Ref. [57]. For the renormalization of the squark sector we follow $\mathcal{O}2$ in Refs. [51,52] (see also Ref. [53]) and for the slepton sector we created an additional $\overline{\text{DR}}$ type version in full analogy to the squark sector.[3] In the following we list these new formulas we used in this analysis.

In the absence of non-minimal flavor violation, the sfermion mass matrix is given by [3,4]

$$\mathbf{M}_{\tilde{f}_{tg}}^2 = \begin{pmatrix} (\mathbf{M}_{L,f_t}^2)_{gg} + m_{f_{tg}}^2 & m_{f_{tg}}(\mathbf{X}_{f_t})_{gg}^* \\ m_{f_{tg}}(\mathbf{X}_{f_t})_{gg} & (\mathbf{M}_{R,f_t}^2)_{gg} + m_{f_{tg}}^2 \end{pmatrix} \quad (3)$$

---

[3] The main difference between the renormalization in Ref. [57] and the one used in this paper is that we impose a further on-shell renormalization condition for the d_g- and e_g-type sfermion masses, including an explicit restoration of the $SU(2)_L$ relation.

where

$$\mathbf{M}_{L,f_t}^2 = M_Z^2 (I_3^{f_t} - Q_{f_t} s_w^2) c_{2\beta}$$
$$+ \begin{cases} \mathbf{M}_{\tilde{L}}^2 & \text{for left-handed sleptons } (t = 1, 2), \\ \mathbf{M}_{\tilde{Q}}^2 & \text{for left-handed squarks } (t = 3, 4), \end{cases}$$

$$\mathbf{M}_{R,f_t}^2 = M_Z^2 Q_{f_t} s_w^2 c_{2\beta}$$
$$+ \begin{cases} \mathbf{M}_{\tilde{E}}^2 & \text{for right-handed sleptons } (t = 2), \\ \mathbf{M}_{\tilde{U}}^2 & \text{for right-handed } u\text{-type squarks } (t=3), \\ \mathbf{M}_{\tilde{D}}^2 & \text{for right-handed } d\text{-type squarks } (t=4), \end{cases}$$

$$\mathbf{X}_{f_t} = \mathbf{A}_{f_t} - \mu^*$$
$$\times \begin{cases} 1/t_\beta & \text{for isospin-up sfermions } (t = 3), \\ t_\beta & \text{for isospin-down sfermions } (t = 2, 4). \end{cases}$$

The soft-SUSY-breaking parameters $\mathbf{M}_{\tilde{L},\tilde{Q},\tilde{E},\tilde{U},\tilde{D}}^2$ and $\mathbf{A}_f$ are 3×3 matrices in flavor space whose off-diagonal entries are zero in the minimally flavor-violating MSSM. Q_f and I_3^f denote the charge and the weak iso-spin of the corresponding fermion, and $c_{2\beta} \equiv \cos 2\beta$.

The mass matrix is diagonalized by a unitary transformation $\mathbf{U}_{\tilde{f}}$,

$$\mathbf{U}_{\tilde{f}} \mathbf{M}_{\tilde{f}}^2 \mathbf{U}_{\tilde{f}}^\dagger = \begin{pmatrix} m_{\tilde{f}_1}^2 & 0 \\ 0 & m_{\tilde{f}_2}^2 \end{pmatrix}, \quad \mathbf{U}_{\tilde{f}} = \begin{pmatrix} U_{11}^{\tilde{f}} & U_{12}^{\tilde{f}} \\ U_{21}^{\tilde{f}} & U_{22}^{\tilde{f}} \end{pmatrix}. \quad (4)$$

We renormalize the up-type squarks ($\tilde{u}_{\{g=1,2,3\}} = \{\tilde{u}, \tilde{c}, \tilde{t}\}$) and the sneutrinos ($\tilde{\nu}_{\{g=1,2,3\}} = \{\tilde{\nu}_e, \tilde{\nu}_\mu, \tilde{\nu}_\tau\}$) on-shell (OS). For the down-type squarks ($\tilde{d}_{\{g=1,2,3\}} = \{\tilde{d}, \tilde{s}, \tilde{b}\}$) and the electron-type sleptons ($\tilde{e}_{\{g=1,2,3\}} = \{\tilde{e}, \tilde{\mu}, \tilde{\tau}\}$) we follow the discussion in Sect. 4 (option $\mathcal{O}2$) of Refs. [51,52] and renormalize them on-shell. They then have to be computed from a mass matrix with shifted $M_{\tilde{L}}^2$, $M_{\tilde{Q}}^2$, $M_{\tilde{E}}^2$ and $M_{\tilde{D}}^2$; see below.

We apply the "m_b, A_b $\overline{\text{DR}}$" scheme of Refs. [51–53]. The scheme affecting sfermions $\tilde{e}_g$, $\tilde{d}_g$ is chosen with the variable $SfScheme[t, g]$:

$SfScheme[2, g] = DR[2]$
    mixed scheme with $m_{\tilde{e}_{2g}}$ OS, $A_{e_g} \overline{\text{DR}}$,   (5a)

$SfScheme[4, g] = DR[2]$
    mixed scheme with $m_{\tilde{d}_{2g}}$ OS, $A_{d_g} \overline{\text{DR}}$.   (5b)

In the following, the sfermion index s runs over both values 1, 2. All sfermions are on-shell,

$$\texttt{dMSfsq1[1,1,1,g]} \equiv \delta m_{\tilde{\nu}_{1g}}^2 = \widetilde{\text{Re}}\big(\Sigma_{\tilde{\nu}_g}(m_{\tilde{\nu}_{1g}}^2)\big)_{11}, \quad (6a)$$

$$\texttt{dMSfsq1[s,s,2,g]} \equiv \delta m_{\tilde{e}_{sg}}^2 = \widetilde{\text{Re}}\big(\Sigma_{\tilde{e}_g}(m_{\tilde{e}_{sg}}^2)\big)_{ss}, \quad (6b)$$

$$\texttt{dMSfsq1[s,s,3,g]} \equiv \delta m_{\tilde{u}_{sg}}^2 = \widetilde{\text{Re}}\big(\Sigma_{\tilde{u}_g}(m_{\tilde{u}_{sg}}^2)\big)_{ss}, \quad (6c)$$

`dMSfsq1[s, s, 4, g]` $\equiv \delta m^2_{\tilde{d}_{sg}} = \widetilde{\mathrm{Re}}\big(\Sigma_{\tilde{d}_g}(m^2_{\tilde{d}_{sg}})\big)_{ss}.$

$$(6d)$$

The up-type off-diagonal mass-matrix entries receive counterterms [51,52,58,59]

`dMSfsq1[1, 2, 3, g]` $\equiv \delta Y_{u_g}$

$$= \frac{1}{2}\widetilde{\mathrm{Re}}\big(\Sigma_{\tilde{u}_g}(m^2_{\tilde{u}_{1g}}) + \Sigma_{\tilde{u}_g}(m^2_{\tilde{u}_{2g}})\big)_{12},$$

$$(7a)$$

`dMSfsq1[2, 1, 3, g]` $\equiv \delta Y^*_{u_g}$

$$= \frac{1}{2}\widetilde{\mathrm{Re}}\big(\Sigma_{\tilde{u}_g}(m^2_{\tilde{u}_{1g}}) + \Sigma_{\tilde{u}_g}(m^2_{\tilde{u}_{2g}})\big)_{21}.$$

$$(7b)$$

For clarity of notation we furthermore define the auxiliary constants

`dMsq12Sf1[2, g]` $\equiv \delta M^2_{\tilde{e}_g,12} = m_{e_g}(\delta A^*_{e_g} - \mu\,\delta t_\beta - t_\beta\,\delta\mu)$

$$+ (A^*_{e_g} - \mu\,t_\beta)\,\delta m_{e_g},$$

$$(8)$$

`dMsq12Sf1[4, g]` $\equiv \delta M^2_{\tilde{d}_g,12} = m_{d_g}(\delta A^*_{d_g} - \mu\,\delta t_\beta - t_\beta\,\delta\mu)$

$$+ (A^*_{d_g} - \mu\,t_\beta)\,\delta m_{d_g}.$$

$$(9)$$

The electron/down-type off-diagonal mass counterterms are related by

`dMSfsq1[1, 2, 2, g]` $\equiv \delta Y_{e_g}$

$$= \frac{1}{|U^{\tilde{e}_g}_{11}|^2 - |U^{\tilde{e}_g}_{12}|^2}\Big\{ U^{\tilde{e}_g}_{11}U^{\tilde{e}_g*}_{21}\big(\delta m^2_{\tilde{e}_{1g}} - \delta m^2_{\tilde{e}_{2g}}\big)$$

$$+ U^{\tilde{e}_g}_{11}U^{\tilde{e}_g*}_{22}\delta M^2_{\tilde{e}_g,12} - U^{\tilde{e}_g}_{12}U^{\tilde{e}_g*}_{21}\delta M^{2*}_{\tilde{e}_g,12}\Big\},$$

$$(10a)$$

`dMSfsq1[2, 1, 2, g]` $\equiv \delta Y^*_{e_g},$

$$(10b)$$

`dMSfsq1[1, 2, 4, g]` $\equiv \delta Y_{d_g}$

$$= \frac{1}{|U^{\tilde{d}_g}_{11}|^2 - |U^{\tilde{d}_g}_{12}|^2}\Big\{ U^{\tilde{d}_g}_{11}U^{\tilde{d}_g*}_{21}\big(\delta m^2_{\tilde{d}_{1g}} - \delta m^2_{\tilde{d}_{2g}}\big)$$

$$+ U^{\tilde{d}_g}_{11}U^{\tilde{d}_g*}_{22}\delta M^2_{\tilde{d}_g,12} - U^{\tilde{d}_g}_{12}U^{\tilde{d}_g*}_{21}\delta M^{2*}_{\tilde{d}_g,12}\Big\},$$

$$(10c)$$

`dMSfsq1[2, 1, 4, g]` $= \delta Y^*_{d_g}.$

$$(10d)$$

The trilinear couplings $A_{f_{tg}} \equiv (\mathbf{A}_{f_t})_{gg}$ are renormalized by

`dAf1[2, g, g]` $\equiv \delta A_{e_g} = \Big\{ \frac{1}{m_{e_g}}\Big[U^{\tilde{e}_g}_{11}U^{\tilde{e}_g*}_{12}(\delta m^2_{\tilde{e}_{1g}} - \delta m^2_{\tilde{e}_{2g}})$

$$+ U^{\tilde{e}_g}_{11}U^{\tilde{e}_g*}_{22}\delta Y^*_{e_g} + U^{\tilde{e}_g*}_{21}U^{\tilde{e}_g}_{21}\delta Y_{e_g} - (A_{e_g} - \mu^* t_\beta)\,\delta m_{e_g}\Big]$$

$$+ \delta\mu^* t_\beta + \mu^* \delta t_\beta\Big\}_{\mathrm{div}},$$

$$(11a)$$

`dAf1[3, g, g]` $\equiv \delta A_{u_g} = \frac{1}{m_{u_g}}\Big[U^{\tilde{u}_g}_{11}U^{\tilde{u}_g*}_{12}(\delta m^2_{\tilde{u}_{1g}} - \delta m^2_{\tilde{u}_{2g}})$

$$+ U^{\tilde{u}_g}_{11}U^{\tilde{u}_g*}_{22}\delta Y^*_{u_g} + U^{\tilde{u}_g*}_{12}U^{\tilde{u}_g}_{21}\delta Y_{u_g} - (A_{u_g} - \mu^*/t_\beta)\,\delta m_{u_g}\Big]$$

$$+ \delta\mu^*/t_\beta - \mu^*\delta t_\beta/t^2_\beta,$$

$$(11b)$$

`dAf1[4, g, g]` $\equiv \delta A_{d_g} = \Big\{ \frac{1}{m_{d_g}}\Big[U^{\tilde{d}_g}_{11}U^{\tilde{d}_g*}_{12}(\delta m^2_{\tilde{d}_{1g}} - \delta m^2_{\tilde{d}_{2g}})$

$$+ U^{\tilde{d}_g}_{11}U^{\tilde{d}_g*}_{22}\delta Y^*_{d_g} + U^{\tilde{d}_g*}_{12}U^{\tilde{d}_g}_{21}\delta Y_{d_g} - (A_{d_g} - \mu^* t_\beta)\,\delta m_{d_g}\Big]$$

$$+ \delta\mu^* t_\beta + \mu^*\delta t_\beta\Big\}_{\mathrm{div}},$$

$$(11c)$$

where the subscripted "div" means to take the divergent part, to effect $\overline{\mathrm{DR}}$ renormalization of A_{e_g} and A_{d_g} [51,52].

As now all the sfermion masses are renormalized as on-shell an explicit restoration of the $SU(2)$ relation is needed. This is performed in requiring that the left-handed (bare) soft SUSY-breaking mass parameter $M_{\tilde{Q}}$ ($M_{\tilde{L}}$) is the same in the $\tilde{d}_g$ ($\tilde{e}_g$) as in the $\tilde{u}_g$ ($\tilde{\nu}_g$) sfermion sector at the one-loop level (see also Refs. [60–63]),

$$M^2_{\tilde{L}}(\tilde{e}_g) = M^2_{\tilde{L}}(\tilde{\nu}_g) + \delta M^2_{\tilde{L}}(\tilde{\nu}_g) - \delta M^2_{\tilde{L}}(\tilde{e}_g),$$

$$(12a)$$

$$M^2_{\tilde{Q}}(\tilde{d}_g) = M^2_{\tilde{Q}}(\tilde{u}_g) + \delta M^2_{\tilde{Q}}(\tilde{u}_g) - \delta M^2_{\tilde{Q}}(\tilde{d}_g)$$

$$(12b)$$

with

$$\delta M^2_{\tilde{L},\tilde{Q}}(\tilde{f}_g) = |U^{\tilde{f}_g}_{11}|^2\delta m^2_{\tilde{f}_{1g}} + |U^{\tilde{f}_g}_{12}|^2\delta m^2_{\tilde{f}_{2g}} - U^{\tilde{f}_g}_{22}U^{\tilde{f}_g*}_{12}\delta Y_{f_g}$$

$$- U^{\tilde{f}_g}_{12}U^{\tilde{f}_g*}_{22}\delta Y^*_{f_g} - 2m_{f_g}\delta m_{f_g}$$

$$+ M^2_Z c_{2\beta} Q_{f_g}, \delta s^2_{\mathrm{w}} - (I^{f_g}_3 - Q_{f_g}s^2_{\mathrm{w}})$$

$$\times (c_{2\beta}\delta M^2_Z + M^2_Z \delta c_{2\beta}).$$

$$(13)$$

Now $M^2_{\tilde{L}}(\tilde{e}_g)$ and $M^2_{\tilde{Q}}(\tilde{d}_g)$ are used in the scalar mass matrix instead of the parameters $M^2_{\tilde{L},\tilde{Q}}$ in Eq. (3) when calculating the values of $m_{\tilde{e}_{sg}}$ and $m_{\tilde{d}_{sg}}$. However, with this procedure, also $m_{\tilde{e}_{2g}}$ and $m_{\tilde{d}_{2g}}$ are shifted, which contradicts our choice of independent parameters. To keep this choice, also the right-handed soft SUSY-breaking mass parameters $M^2_{\tilde{E},\tilde{D}}$ receive a shift:[4]

$$M^2_{\tilde{E}}(\tilde{e}_g) = \frac{m^2_{e_g}|X_{e_g}|^2}{M^2_{\tilde{L}}(\tilde{e}_g) + m^2_{e_g} + c_{2\beta}M^2_Z(I^e_3 - Q_e s^2_{\mathrm{w}}) - m^2_{\tilde{e}_{2g}}}$$

$$- m^2_{e_g} - c_{2\beta}M^2_Z Q_e s^2_{\mathrm{w}} + m^2_{\tilde{e}_{2g}},$$

$$(14a)$$

---

[4] If the mass of the $\tilde{d}_{1g}$ ($\tilde{e}_{1g}$) sfermion is chosen as independent mass as $\tilde{d}_{2g} \approx \tilde{d}_{Lg}$ ($\tilde{e}_{2g} \approx \tilde{e}_{Lg}$) then the shift of $M^2_{\tilde{D}}$ ($M^2_{\tilde{E}}$) has to be performed with respect to $m_{\tilde{d}_{1g}}$ ($m_{\tilde{e}_{1g}}$).

$$M_{\tilde{D}}^2(\tilde{d}_g) = \frac{m_{d_g}^2 |X_{d_g}|^2}{M_{\tilde{Q}}^2(\tilde{d}_g) + m_{d_g}^2 + c_{2\beta} M_Z^2 (I_3^d - Q_d s_w^2) - m_{\tilde{d}_{2g}}^2}$$
$$- m_{d_g}^2 - c_{2\beta} M_Z^2 Q_d s_w^2 + m_{\tilde{d}_{2g}}^2. \tag{14b}$$

Taking into account this shift in $M_{\tilde{E},\tilde{D}}^2$, up to one-loop order,[5] the *new* resulting mass parameters $m_{\tilde{e}_{1g}}$ and $m_{\tilde{d}_{1g}}$ are the same as the on-shell masses

$$\left(m_{\tilde{e}_{1g}}^{\rm OS}\right)^2 = m_{\tilde{e}_{1g}}^2 + \delta m_{\tilde{e}_{1g}}^2 - \widetilde{\rm Re}\left(\Sigma_{\tilde{e}_g}(m_{\tilde{e}_{1g}}^2)\right)_{11}, \tag{15a}$$

$$\left(m_{\tilde{d}_{1g}}^{\rm OS}\right)^2 = m_{\tilde{d}_{1g}}^2 + \delta m_{\tilde{d}_{1g}}^2 - \widetilde{\rm Re}\left(\Sigma_{\tilde{d}_g}(m_{\tilde{d}_{1g}}^2)\right)_{11}. \tag{15b}$$

The input parameters in the $b/\tilde{b}$ sector have to correspond to the chosen renormalization. We start by defining the bottom mass, where the experimental input is the SM $\overline{\rm MS}$ mass [66],

$$m_b^{\overline{\rm MS}}(m_b) = 4.18 \text{ GeV}. \tag{16}$$

To convert to the $\overline{\rm DR}$ mass the following procedure is chosen. The value of $m_b^{\overline{\rm MS}}(\mu_R)$ (at the renormalization scale μ_R) is calculated from $m_b^{\overline{\rm MS}}(m_b)$ at the three-loop level

$$m_b^{\overline{\rm MS}}(\mu_R) = m_b^{\overline{\rm MS}}(m_b) \frac{c(\alpha_s^{\overline{\rm MS},(n_f)}(\mu_R)/\pi)}{c(\alpha_s^{\overline{\rm MS},(n_f)}(m_b)/\pi)} \tag{17}$$

via the function $c(x)$ following the prescription given in Refs. [67,68]. n_f denotes the number of active flavors. The "on-shell" mass is connected to the $\overline{\rm MS}$ mass via

$$m_b^{\rm os} = m_b^{\overline{\rm MS}}(\mu_R)$$
$$\times \left[1 + \frac{\alpha_s^{\overline{\rm MS},(n_f)}(\mu_R)}{\pi}\left(\frac{4}{3} + 2\ln\frac{\mu_R}{m_b^{\overline{\rm MS}}(\mu_R)}\right) + \cdots\right], \tag{18}$$

where the ellipsis denote the two- and three-loop contributions, which can also be found in Refs. [67,68]. The $\overline{\rm DR}$ bottom quark mass at the scale μ_R is calculated iteratively from [59,65,69]

$$m_b^{\overline{\rm DR}} = m_b^{\rm os} + \frac{\delta m_b^{\rm OS} - \delta m_b^{\overline{\rm DR}}}{|1 + \Delta_b|} \tag{19}$$

with an accuracy of $|1 - (m_b^{\overline{\rm DR}})^{(n)}/(m_b^{\overline{\rm DR}})^{(n-1)}| < 10^{-5}$ reached in the nth step of the iteration.

The quantity Δ_b [25,69–72] (see also Ref. [73]) resums the $\mathcal{O}((\alpha_s t_\beta)^n)$ and $\mathcal{O}((\alpha_t t_\beta)^n)$ terms and is given by

$$\Delta_b = -\frac{\mu^* t_\beta}{\pi}\left[\frac{2}{3}\alpha_s(m_t) M_3^* I(m_{\tilde{b}_1}^2, m_{\tilde{b}_2}^2, m_{\tilde{g}}^2)\right.$$
$$\left. + \frac{1}{4}\alpha_t(m_t) A_t^* I(m_{\tilde{t}_1}^2, m_{\tilde{t}_2}^2, |\mu|^2)\right] \tag{20}$$

with

$$I(a, b, c) = C_0(0, 0, 0, a, b, c)$$
$$= -\frac{ab\ln(b/a) + ac\ln(a/c) + bc\ln(c/b)}{(c-a)(c-b)(b-a)}. \tag{21}$$

Here α_t is defined in terms of the top Yukawa coupling $y_t(m_t) = \sqrt{2}m_t(m_t)/v$ as $\alpha_t(m_t) = y_t^2(m_t)/(4\pi)$ with $v = 1/\sqrt{\sqrt{2}\,G_F} = 246.218$ GeV, and $m_t(m_t) \approx m_t/(1 - \frac{1}{2\pi}\alpha_t(m_t) + \frac{4}{3\pi}\alpha_s(m_t))$. Setting in the evaluation of Δ_b the scale to m_t was shown to yield in general a more stable result [22,23] as long as two-loop corrections to Δ_b are not included.[6] M_3 is the soft SUSY-breaking parameter for the gluinos. We have neglected any CKM mixing of the quarks.

The Z factors of the squark fields are derived in the OS scheme. They can be found in Ref. [57].

2.5 The strong coupling constant

The decoupling of the heavy particles and the running is taken into account in the definition of α_s: the starting point is [66]

$$\alpha_s^{\overline{\rm MS},(5)}(M_Z) = 0.1184, \tag{22}$$

where the running of $\alpha_s^{\overline{\rm MS},(n_f)}(\mu_R)$ can be found in Ref. [66]. μ_R denotes the renormalization scale, which is typically of the order of the energy scale of the considered process.

From the $\overline{\rm MS}$ value the $\overline{\rm DR}$ value is obtained at the two-loop level via the phenomenological one-step formula [74, 75]

$$\alpha_s^{\overline{\rm DR},(n_f)}(\mu_R) = \alpha_s^{\overline{\rm MS},(n_f)}(\mu_R)\left\{1 + \frac{\alpha_s^{\overline{\rm MS},(n_f)}(\mu_R)}{\pi}\right.$$
$$\times \left(\frac{1}{4} - \zeta_1^{(n_f)}\right) + \left(\frac{\alpha_s^{\overline{\rm MS},(n_f)}(\mu_R)}{\pi}\right)^2$$
$$\left. \times \left[\frac{11}{8} - \frac{n_f}{12} - \frac{1}{2}\zeta_1^{(n_f)} + 2(\zeta_1^{(n_f)})^2 - \zeta_2^{(n_f)}\right]\right\}, \tag{23}$$

---

[5] In the case of a pure OS scheme (see e.g. [64,65] for the rMSSM) the shifts Eqs. (12) and (14) result in mass parameters $m_{\tilde{d}_{1g}}$ and $m_{\tilde{e}_{1g}}$, which are exactly the same as in Eq. (15). This constitutes an important consistency check of these two different methods.

[6] It should be noted that in Refs. [22,23] a different scale has been advocated due to the emphasis on the two-loop contributions presented in this paper. The plots, however, show that m_t is a good scale choice if only one-loop corrections are included.
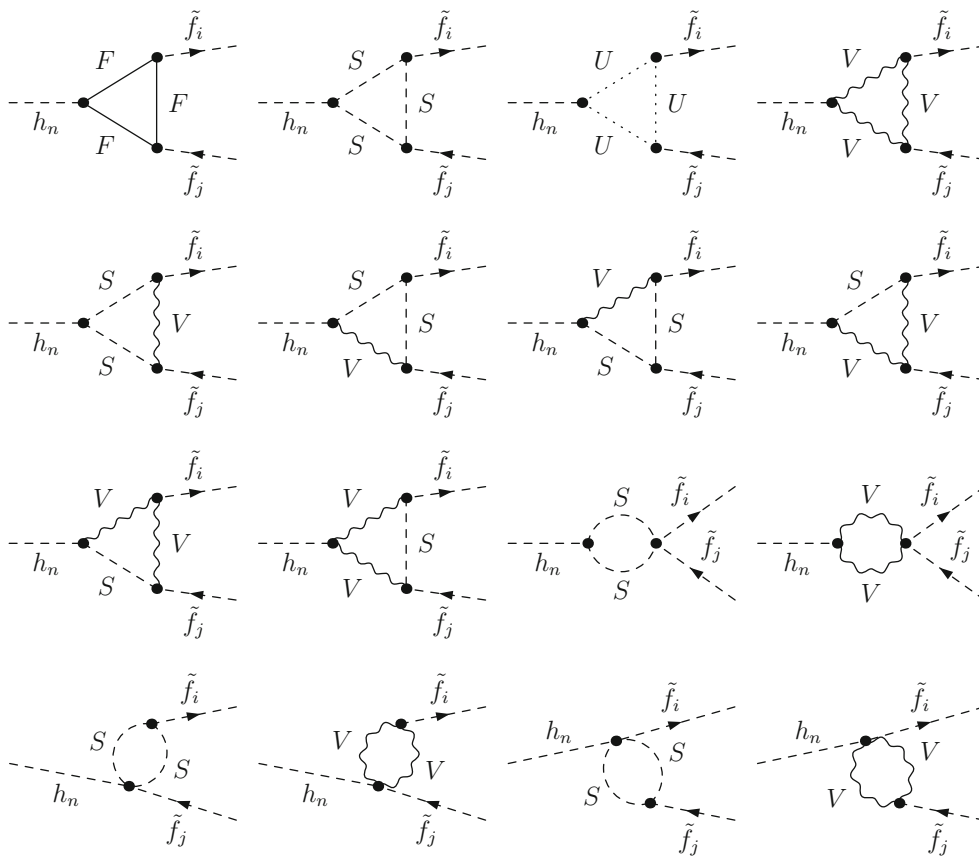
Fig. 1 Generic Feynman diagrams for the decay $h_n \rightarrow \tilde{f}_i \tilde{f}_j$ ($n = 2, 3$; $i, j = 1, 2$). F can be a SM fermion, chargino, neutralino, or gluino; S can be a sfermion or a Higgs/Goldstone boson; U denotes the ghosts; V can be a γ, Z, $W^{\pm}$, or g. Not shown are the diagrams with a h_n–Z or h_n–G transition contribution on the external Higgs-boson leg

where (for $n_f = 6$)

$$\zeta_1^{(6)} = -\ln \frac{\mu_R^2}{\tilde{M}^2}, \quad \zeta_2^{(6)} = -\frac{65}{32} - \frac{5}{2} \ln \frac{\mu_R^2}{\tilde{M}^2} + \left(\ln \frac{\mu_R^2}{\tilde{M}^2} \right)^2,$$

(24)

with $\tilde{M}^2$ being defined as the geometric average of all squark masses multiplied with the gluino mass,[7] $\tilde{M}^2 = m_{\tilde{g}} \prod_{\tilde{q}} (m_{\tilde{q}_1} m_{\tilde{q}_2})^{\frac{1}{12}}$. The log terms originates from the decoupling of the SQCD particles from the running of α_s at lower scales $\mu_R \leq \mu_{\text{dec}}$. Here μ_{dec} denotes the decoupling scale for heavy particles, i.e. the scale where intermediate effective theories are introduced by integrating out the heavy degrees of freedom. For simplification we have chosen the energy scale of the considered processes (as a typical SUSY scale) also as decoupling scale.

3 Calculation of loop diagrams

In this section we give some details about the calculation of the higher-order corrections to the partial decay widths of Higgs bosons. Sample diagrams are shown in Figs. 1 and 2. Not shown are the diagrams for real (hard and soft) photon and gluon radiation. They are obtained from the corresponding tree-level diagrams by attaching a photon (gluon) to the electrically (color) charged particles. The internal generically depicted particles in Figs. 1 and 2 are labeled as follows: F can be a SM fermion f, chargino $\tilde{\chi}_j^{\pm}$, neutralino $\tilde{\chi}_k^0$, or gluino $\tilde{g}$; S can be a sfermion $\tilde{f}_i$ or a Higgs (Goldstone) boson h_n (G); U denotes the ghosts u_V; V can be a photon γ, gluon g, or a massive SM gauge boson, Z or $W^{\pm}$. For internally appearing Higgs bosons no higher-order corrections to their masses or couplings are taken into account; these corrections would correspond to effects beyond one-loop order.[8] For external Higgs bosons, as described in Sect. 2.1,

---

[7] $\tilde{M}$ is chosen such that $\ln \frac{m_{\tilde{g}}^2}{\tilde{M}^2} + \frac{1}{6} \sum_{\tilde{q}} \ln \frac{m_{\tilde{q}_1} m_{\tilde{q}_2}}{\tilde{M}^2} = 0$, which means that the corresponding diagrams vanish at zero momentum transfer. Under this condition $\alpha_s(\mu_R)$ is well defined.

[8] We found that using loop corrected Higgs-boson masses in the loops leads to a UV divergent result.
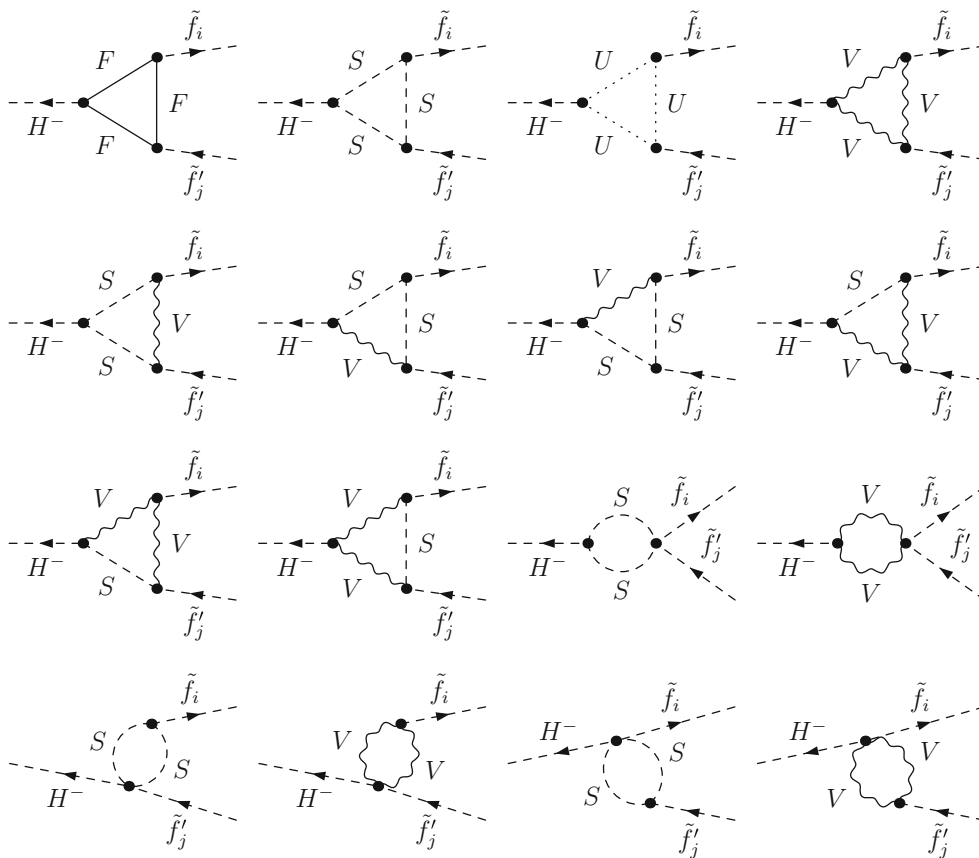
Fig. 2 Generic Feynman diagrams for the decay $H^+ \to \tilde{f}_i \tilde{f}'_j$ ($i, j = 1, 2$). (It should be noted that all *arrows* are inverted in case of a H^- decay.) F can be a SM fermion, chargino, neutralino, or gluino; S can be a sfermion or a Higgs/Goldstone boson; U denotes the ghosts; V can be a γ, Z, $W^{\pm}$, or g. Not shown are the diagrams with a $H^{\pm}$–$W^{\pm}$ or $H^{\pm}$–$G^{\pm}$ transition contribution on the external Higgs-boson leg

the appropriate $\hat{Z}$ factors are applied and on-shell masses (including higher-order corrections) are used [33], obtained with FeynHiggs [33–38].

Also not shown are the diagrams with a Higgs–gauge/Goldstone boson self-energy contribution on the external Higgs-boson leg. They appear in the decay $h_n \to \tilde{f}_i \tilde{f}_j$, Fig. 1, with a h_n–Z/G transition and in the decay $H^{\pm} \to \tilde{f}_i \tilde{f}'_j$, Fig. 2, with a $H^{\pm}$–$W^{\pm}/G^{\pm}$ transition.[9]

Furthermore, in general, in Figs. 1 and 2 we have omitted diagrams with self-energy type corrections of external (on-shell) particles. While the contributions from the real parts of the loop functions are taken into account via the renormalization constants defined by on-shell renormalization conditions, the contributions coming from the imaginary part of the loop functions can result in an additional (real) correction if multiplied by complex parameters (such as A_f). In the analytical and numerical evaluation, these diagrams have

been taken into account via the prescription described in Ref. [57].

Within our one-loop calculation we neglect finite width effects that can help to cure threshold singularities. Consequently, in the close vicinity of those thresholds our calculation does not give a reliable result. Switching to a complex mass scheme [76] would be another possibility to cure this problem, but its application is beyond the scope of our paper.

The diagrams and corresponding amplitudes have been obtained with FeynArts [77–79]. The model file, including the MSSM counterterms, is largely based on Ref. [57]; however, adjusted to match exactly the renormalization prescription described in Sect. 2. The further evaluation has been performed with FormCalc and LoopTools [80].

3.1 Ultraviolet divergences

As regularization scheme for the UV divergences we have used constrained differential renormalization [81], which has been shown to be equivalent to dimensional reduction [82,83] at the one-loop level [80]. Thus the employed regulariza-

---

[9] From a technical point of view, the $H^{\pm}$–$W^{\pm}/G^{\pm}$ transitions have been absorbed into the respective counterterms, while the h_n–Z/G transitions have been calculated explicitly.

tion scheme preserves SUSY [84,85] and guarantees that the SUSY relations are kept intact, e.g. that the gauge couplings of the SM vertices and the Yukawa couplings of the corresponding SUSY vertices also coincide to one-loop order in the SUSY limit. Therefore no additional shifts, which might occur when using a different regularization scheme, arise. All UV divergences cancel in the final result.

3.2 Infrared divergences

The IR divergences from diagrams with an internal photon or gluon have to cancel with the ones from the corresponding real soft radiation. In the case of QED we have included the soft photon contribution following the description given in Ref. [86]. In the case of QCD we have modified this prescription by replacing the product of electric charges by the appropriate combination of color charges (linear combination of C_A and C_F times α_s).

The IR divergences arising from the diagrams involving a γ (or a g) are regularized by introducing a photon (or gluon) mass parameter, λ. While for the QED part this procedure always works, in the QCD part due to its non-Abelian character this method can fail. However, since no triple or quartic gluon vertices appear, λ can indeed be used as a regulator. Using shifted (i.e. on-shell) sfermion masses inside tree- *and* loop-level calculations guarantees that all IR divergences, i.e. all divergences in the limit $\lambda \to 0$, cancel once virtual and real diagrams for one decay channel are added.

3.3 Tree-level formulas

For completeness we show here also the formulas that have been used to calculate the tree-level decay widths:

$$\Gamma^{\text{tree}}(h_n \to \tilde{f}_i \tilde{f}_j) = \frac{|C(h_n, \tilde{f}_i, \tilde{f}_j)|^2 \, \lambda^{1/2}(m^2_{h_n}, m^2_{\tilde{f}_i}, m^2_{\tilde{f}_j})}{16 \, \pi \, m^3_{h_n}}$$
$$\times \, (n = 2, 3; \; i, j = 1, 2), \qquad (25)$$

$$\Gamma^{\text{tree}}(H^\pm \to \tilde{f}_i \tilde{f}'_j) = \frac{|C(H^\pm, \tilde{f}_i, \tilde{f}'_j)|^2 \, \lambda^{1/2}(M^2_{H^\pm}, m^2_{\tilde{f}_i}, m^2_{\tilde{f}'_j})}{16 \, \pi \, M^3_{H^\pm}}$$
$$\times \, (i, j = 1, 2), \qquad (26)$$

where $\lambda(x, y, z) = (x - y - z)^2 - 4yz$ and the couplings $C(a, b, c)$ can be found in the FeynArts model files [87].

4 Numerical analysis

In this section we present the comparisons with results from other groups and our numerical analysis of all heavy Higgs-boson decay channels into the third generation sfermions in the cMSSM. In the various figures below we show the partial decay widths and their relative correction at the tree level

("tree") and at the one-loop level ("full"). In addition we show the SQCD corrections ("SQCD") for comparison with the full one-loop result.

4.1 Comparisons

We performed exhaustive comparisons with results from other groups for heavy Higgs-boson decays. Since loop corrections in the MSSM with complex parameters have been evaluated in this work for the first time, these comparisons were restricted to the MSSM with real parameters.

- We calculated the decays $\Phi \to \tilde{q}_i \tilde{q}_j$ at $\mathcal{O}(\alpha_s)$ (Φ denotes any heavy MSSM Higgs boson) and found good agreement with Ref. [55], where only a small difference remains due to the slightly different renormalization schemes. We successfully reproduced their figures, except their Fig. 4 ($H^+ \to \tilde{t}_1 \tilde{b}_1$), which differs substantially. Unfortunately, 17 years after publication, the source code of Ref. [55] is unavailable for a direct comparison [88]. On the other hand our results for $H^+ \to \tilde{t}_1 \tilde{b}_1$ are in good qualitative agreement with Ref. [46]; see below.

- A comparison with Ref. [56] at $\mathcal{O}(\alpha_s)$ was rather difficult. Reference [56] used running $\overline{\text{MS}}$ input parameters and significant differences exist w.r.t. our treatment of the renormalization of the scalar quark sector. Nevertheless, using their input parameters as far as possible, we found qualitative agreement.

- We performed a detailed comparison with Ref. [44] for the decay $H^+ \to \tilde{t}_i \tilde{b}_j$ at $\mathcal{O}(\alpha_s)$. They also differ in the renormalization of the scalar quark sector, leading to different loop corrections. Furthermore, they used tree/$\overline{\text{DR}}$/pole squark masses in tree/loop/phase space. Despite these complications we found rather good qualitative agreement with their Fig. 2.

- A check with Refs. [45] and [46] at $\mathcal{O}(\alpha_s)$ gave good qualitative agreement, although an effective resummation of the trilinear Higgs-sbottom coupling was used in Ref. [46].

- Decays of the $\mathcal{CP}$-odd Higgs boson A to scalar quarks (in the rMSSM) have been compared with Ref. [47]. Again, using their input parameters as far as possible, we found good (qualitative) agreement with their Figs. 4–7.

- A boson decays into sfermions in the rMSSM have been analyzed in Ref. [48]. As in the latter item we found good (qualitative) agreement, especially for the decay into scalar taus after using our new $\overline{\text{DR}}$ type version for the slepton sector, as described above in Sect. 2.4.

- A numerical comparison with the program HFOLD Ref. [50] at the benchmark point SPS1a‘ (proposed in the SPA project [89]) can be found in Table 1. Only for this point sufficient details about the sfermion masses was

Table 1 Comparison of the 1-loop corrected partial decay widths in 10^{-2} GeV

Process	OS masses		$\overline{\text{DR}}$ masses	
	HFOLD	FeynTools	HFOLD	FeynTools
$H^0 \to \tilde{\tau}_1 \tilde{\tau}_1$	1.8426	2.0855	1.9866	2.2733
$H^0 \to \tilde{\tau}_1 \tilde{\tau}_2$	1.9065	1.9001	1.8187	1.8160
$H^0 \to \tilde{\tau}_2 \tilde{\tau}_2$	0.3506	0.4399	–	–
$H^0 \to \tilde{\nu}_\tau \tilde{\nu}_\tau$ [a]	0.1070	0.1263	0.0869	0.0997
$A^0 \to \tilde{\tau}_1 \tilde{\tau}_2$	2.9686	3.1641	2.8278	3.0212
$H^+ \to \tilde{\nu}_\tau \tilde{\tau}_1$	6.4323	7.0313	6.5677	7.0049
$H^+ \to \tilde{\nu}_\tau \tilde{\tau}_2$	0.1180	0.1613	0.0768	0.1022

[a] It should be noted that in HFOLD an additional factor 1/2 appears in the decay to sneutrinos. We omitted this (wrong) factor in the comparison

available for a numerical comparison. (Unfortunately, for this point only decays to scalar leptons are kinematically allowed.) In Table 1 we show the full one-loop results of HFOLD, using $\overline{\text{DR}}$ masses for the internal and external particles, corresponding to the full $\overline{\text{DR}}$ renormalization used in the code (where the renormalization scale was set to 1 TeV [89]). Our results, labeled FeynTools, are evaluated using our renormalization scheme, but inserting the HFOLD $\overline{\text{DR}}$ masses, and we find overall agreement better than 10 % (in the tree-level results we find more than 10 digits agreement).[10]

HFOLD also offers to switch to (the recommended) OS masses for the external particles. In this case, including in our calculation the shifts to OS masses as described in Sect. 2.4, again with overall agreement between the two calculations roughly at the 10 % level. The numerical difference between the two variants ($\overline{\text{DR}}$ and OS) again is roughly at the 10 % level. The fact that our results differ at the same level in the two schemes indicates that the numerical differences are mostly due to the different renormalization schemes used in our calculation and in HFOLD.

Finally, it should be noted that Refs. [44–48] subsequently had been recompiled in Ref. [49].

4.2 Parameter settings

The renormalization scale μ_R has been set to the mass of the decaying Higgs boson. The SM parameters are chosen as follows; see also [66]:

---

[10] It should be noted that we found results substantially closer to the HFOLD $\overline{\text{DR}}$ result using a "quasi" $\overline{\text{DR}}$ scheme [where "quasi" means that our analytic integrals for the real radiation contain a finite piece and thus cannot easily be matched to pure $\overline{\text{DR}}$ vertex renormalizations (of IR divergent diagrams)].

- Fermion masses (on-shell masses, if not indicated differently):

$$
\begin{aligned}
& m_e = 0.510998928 \text{ MeV}, \quad m_{\nu_e} = 0 \text{ MeV}, \\
& m_\mu = 105.65837515 \text{ MeV}, \quad m_{\nu_\mu} = 0 \text{ MeV}, \\
& m_\tau = 1776.82 \text{ MeV}, \quad m_{\nu_\tau} = 0 \text{ MeV}, \\
& m_u = 68.7 \text{ MeV}, \quad m_d = 68.7 \text{ MeV}, \\
& m_c = 1.275 \text{ GeV}, \quad m_s = 95.0 \text{ MeV}, \\
& m_t = 173.07 \text{ GeV}, \quad m_b = 4.18 \text{ GeV}.
\end{aligned} \tag{27}
$$

According to Ref. [66], m_s is an estimate of a so-called "current quark mass" in the $\overline{\text{MS}}$ scheme at the scale $\mu \approx 2$ GeV. $m_c \equiv m_c(m_c)$ and $m_b \equiv m_b(m_b)$ are the "running" masses in the $\overline{\text{MS}}$ scheme. The top quark mass as well as the lepton masses are defined OS. m_u and m_d are effective parameters, calculated through the hadronic contributions to

$$
\begin{aligned}
\Delta\alpha_{\text{had}}^{(5)}(M_Z) &= \frac{\alpha}{\pi} \sum_{f=u,c,d,s,b} Q_f^2 \left(\ln\frac{M_Z^2}{m_f^2} - \frac{5}{3} \right) \\
&\sim 0.027723.
\end{aligned} \tag{28}
$$

- The CKM matrix has been set to unity.
- Gauge-boson masses:

$$
M_Z = 91.1876 \text{ GeV}, \quad M_W = 80.385 \text{ GeV}. \tag{29}
$$

- Coupling constants:

$$
\alpha(0) = 1/137.0359895, \quad \alpha_s(M_Z) = 0.1184, \tag{30}
$$

where the running and decoupling of α_s is described in Sect. 2.5.

The Higgs sector quantities (masses, mixings, etc.) have been evaluated using FeynHiggs (version 2.10.2) [33–38].

Table 2 MSSM parameters for the initial numerical investigation; all parameters (except of t_β) are in GeV. In our analysis $M_{\tilde{Q}_3}$, $M_{\tilde{U}_3}$, $M_{\tilde{D}_3}$, $M_{\tilde{L}_3}$, and $M_{\tilde{E}_3}$ are chosen such that the values of $m_{\tilde{t}_1}$, $m_{\tilde{t}_2}$, $m_{\tilde{b}_2}$, $m_{\tilde{\nu}_\tau}$, and $m_{\tilde{\tau}_2}$ are realized. For the $\tilde{d}_g$ and $\tilde{e}_g$ sector the shifts in $M_{\tilde{Q},\tilde{D}}(\tilde{d}_g)$ and $M_{\tilde{L},\tilde{E}}(\tilde{e}_g)$ as defined in Eqs. (12) and (14) are taken into account,

concerning $m_{\tilde{t}_1}$ and $m_{\tilde{b}_1}$ (rounded to 1 MeV). The values for A_t, A_b, and A_τ are chosen such that charge- and/or color-breaking minima are avoided [90–96]. It should be noted that for the first and second generation of sfermions we chose instead $M_{\tilde{L},\tilde{E}} = 1500$ GeV and $M_{\tilde{Q},\tilde{U},\tilde{D}} = 2000$ GeV

Scen.	t_β	$m_{\tilde{t}_1}$	$m_{\tilde{t}_2}$	$m_{\tilde{b}_2}$	$m_{\tilde{\nu}_\tau}$	$m_{\tilde{\tau}_2}$	μ	$|A_t|$	$|A_b|$	$|A_\tau|$	M_1	M_2	M_3
S1/S2/S3	10	394	771	582	280	309	500	1200	600	1000	300	600	1500

| Scen.	$M_{H^\pm}$	m_{h_1}	m_{h_2}	m_{h_3}	$m_{\tilde{\tau}_1}$	$m_{\tilde{b}_1}$
S1	1000	123.405	996.766	996.813	282.517	513.289
S2	1400	123.428	1397.299	1398.596	282.337	513.167
S3	1600	123.436	1597.174	1597.524	282.265	513.124
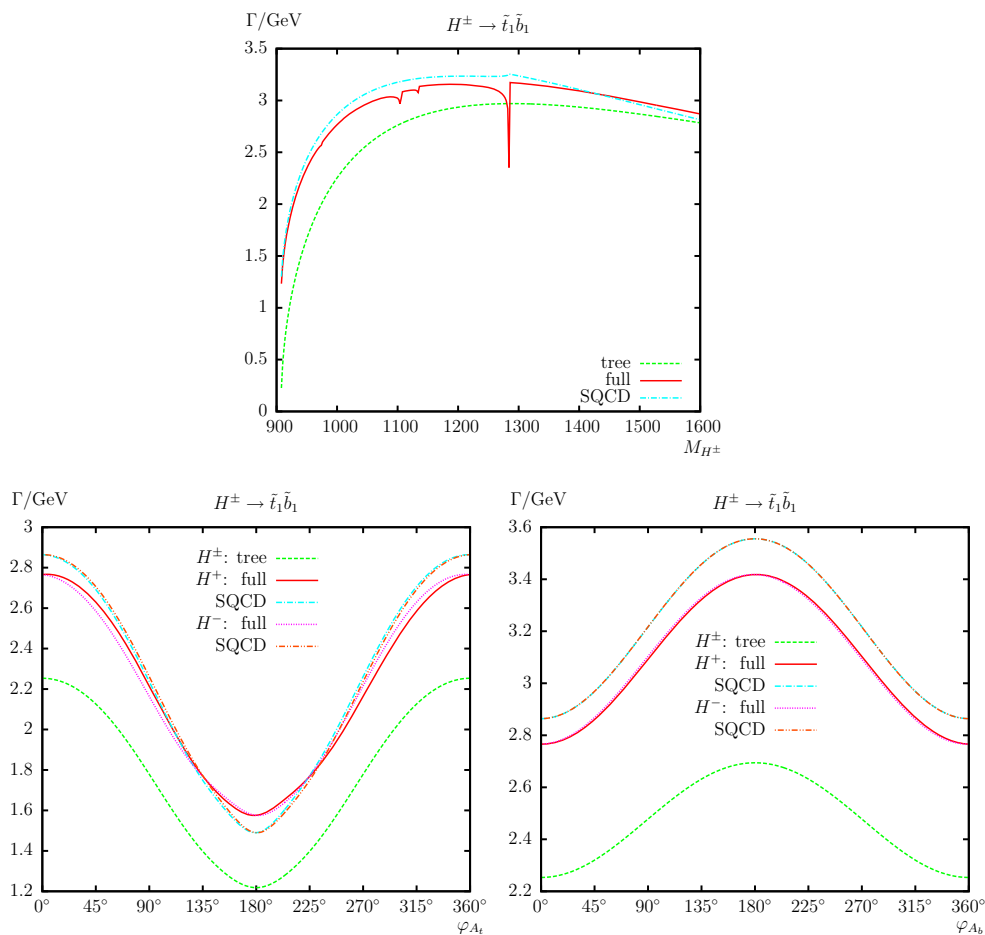
Fig. 3 $\Gamma(H^\pm \to \tilde{t}_1\tilde{b}_1)$. Tree-level, full, and SQCD one-loop corrected partial decay widths are shown. The *upper plot* shows the partial decay width with $M_{H^\pm}$ varied. The *lower plots* show the complex phases φ_{A_t} (left) and φ_{A_b} (right) varied with parameters chosen according to S1 (see Table 2)

Furthermore, the current limits for SUSY particle searches [66] are roughly fulfilled in our analysis.

We emphasize again that the analytical calculation has been done for *all* decays into sfermions, but in the numerical analysis we concentrate on the decays to third generation sfermions. Results are shown for some representative numerical examples. The parameters are chosen according to the scenarios, S1, S2 and S3, shown in Table 2. The scenarios are defined such that a maximum number of (third generation) decay modes are open simultaneously to permit an analysis of all channels, i.e. not picking specific parameters for each decay. For the same reason we do not demand that the lightest Higgs boson has a mass around ~125 GeV, although for most of the parameter space this is given. The
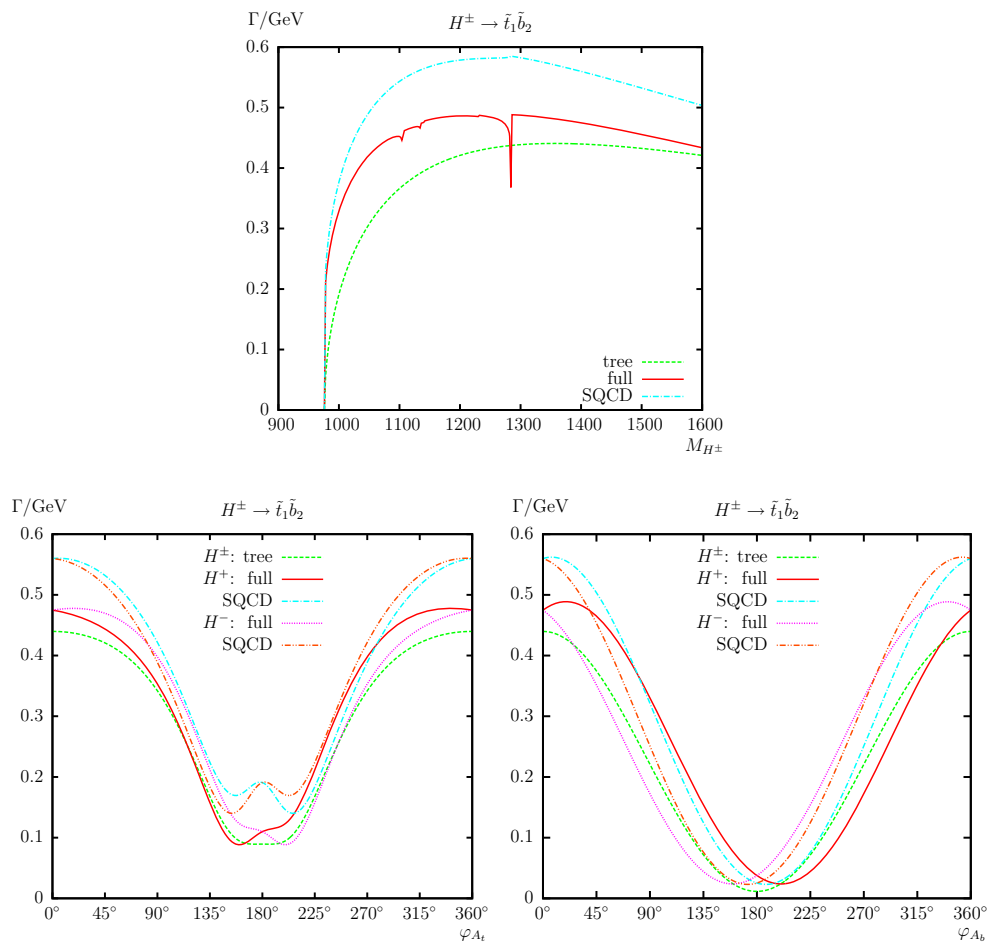
Fig. 4 $\Gamma(H^\pm \to \tilde{t}_1 \tilde{b}_2)$. Tree-level, full, and SQCD one-loop corrected partial decay widths are shown. The *upper plot* shows the partial decay width with $M_{H^\pm}$ varied. The *lower plots* show the complex phases φ_{A_t} (*left*) and φ_{A_b} (*right*) varied with parameters chosen according to S2 (see Table 2)

only parameter varied with a sizable impact on m_{h_1} is φ_{A_t}. For $110° < \varphi_{A_t} < 250°$ the light Higgs-boson mass drops slightly below 122 GeV, but stays above 121 GeV, where a theory uncertainty in the prediction of $\sim$3 GeV [37] must be kept in mind.

The numerical results we will show in the next subsections are of course dependent on choice of the SUSY parameters. Nevertheless, they give an idea of the relevance of the full one-loop corrections. Channels (and their respective one-loop corrections) that may look unobservable due to the smallness of their decay width in the plots shown below, could become important if other channels are kinematically forbidden.

4.3 Full one-loop results for varying $M_{H^\pm}$ and φ_A

The results shown in this and the following subsections consist of "tree", which denotes the tree-level value and of "full", which is the partial decay width including *all* one-loop corrections as described in Sect. 3. Also shown are the pure SUSY-QCD one-loop corrections ("SQCD") for colored decays. We restrict ourselves to the analysis of the decay widths themselves, since the one-loop effects on the branching ratios are strongly parameter dependent, as discussed in the previous subsection.

When performing an analysis involving complex parameters it should be noted that the results for physical observables are affected only by certain combinations of the complex phases of the parameters μ, the trilinear couplings $A_{t,b,\tau}$ and the gaugino mass parameters $M_{1,2,3}$ [97,98]. It is possible, for instance, to rotate the phase φ_{M_2} away. Experimental constraints on the (combinations of) complex phases arise, in particular, from their contributions to electric dipole moments of the electron and the neutron (see Refs. [99–101] and references therein), of the deuteron [102] and of heavy quarks [103,104]. While SM contributions enter only at the three-loop level, due to its complex phases the MSSM can contribute already at one-loop order. Large phases in the first two generations of sfermions can only be accommodated if these generations are assumed to be very heavy [105,106] or large
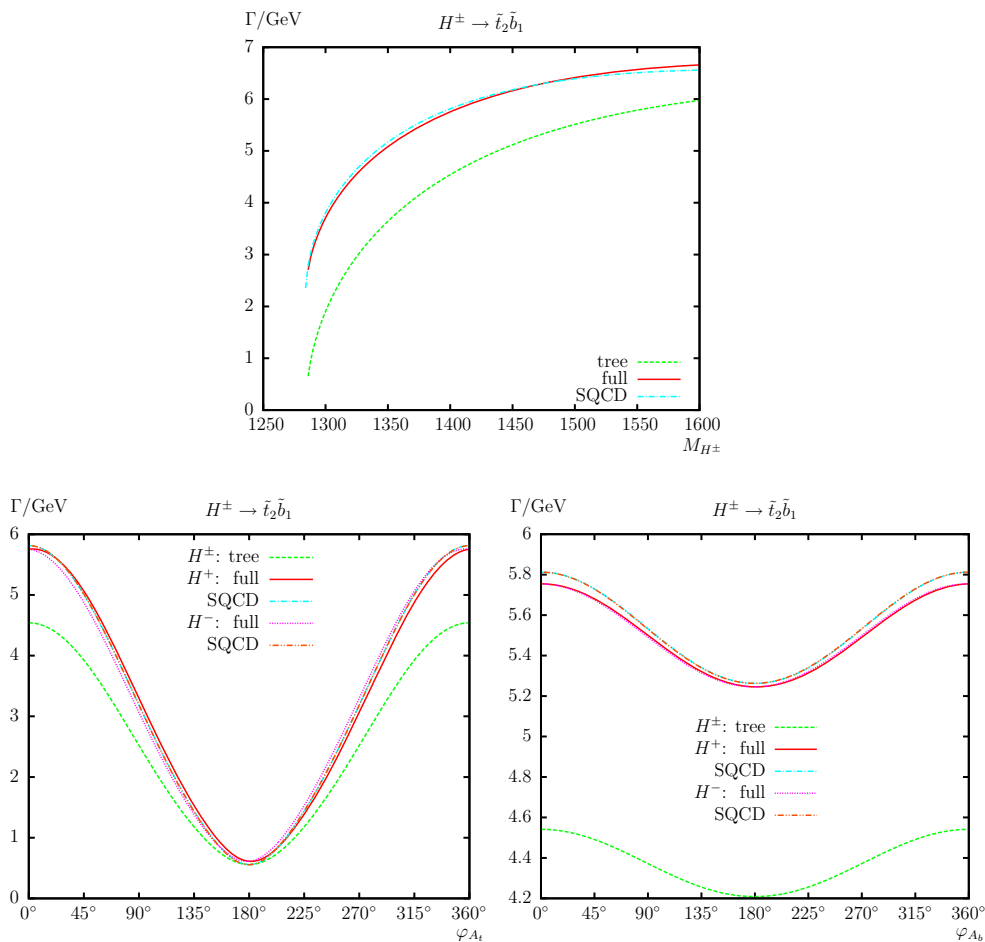
Fig. 5 $\Gamma(H^\pm \to \tilde{t}_2\tilde{b}_1)$. Tree-level, full, and SQCD one-loop corrected partial decay widths are shown. The *upper plot* shows the partial decay width with $M_{H^\pm}$ varied. The *lower plots* show the complex phases φ_{A_t}

(*left*) and φ_{A_b} (*right*) varied with parameters chosen according to S2 (see Table 2)

cancelations occur [107–109]; see, however, the discussion in Ref. [110]. A review can be found in Ref. [111]. Accordingly (using the convention that $\varphi_{M_2} = 0$, as done in this paper), in particular, the phase φ_μ is tightly constrained [112], while the bounds on the phases of the third generation trilinear couplings are much weaker. Setting $\varphi_\mu = \varphi_{M_1} = \varphi_{\tilde{g}} = 0$ leaves us with φ_{A_t}, φ_{A_b}, and φ_{A_τ} as the only complex valued parameters. It should be noted that the tree-level prediction depends on φ_A via the sfermion mixing matrix and the variation of the phases $\varphi_{A_{t,b}}$ (φ_{A_τ}) leads to a maximal change of 10 % (20 %) in the squark (slepton) masses.

Since now complex trilinear A_f parameters can appear in the couplings, contributions from absorptive parts of self-energy type corrections on external legs can arise. The corresponding formulas for an inclusion of these absorptive contributions via finite wave function correction factors can be found in [53,57].

We start the numerical analysis with partial decay widths of $H^\pm$ evaluated as a function of $M_{H^\pm}$, starting at $M_{H^\pm} = $

600 GeV up to $M_{H^\pm} = 1.6$ TeV, which roughly coincides with the reach of the LHC for high-luminosity running as well as an e^+e^- collider with a center-of-mass energy up to $\sqrt{s} \sim$ 3 TeV [15,16]. Then we turn to the h_n ($n = 2, 3$) decays.

4.3.1 $H^\pm$ decays into sfermions

In Figs. 3, 4, 5, 6, 7 and 8 we show the results for the processes $H^\pm \to \tilde{f}_i \tilde{f}'_j$ ($i, j = 1, 2$) as a function of $M_{H^\pm}$ and as a function of the relevant complex phases φ_A. These are of particular interest for LHC analyses [113,114] (as emphasized in Sect. 1). The various visible (or hardly visible) dips and steps occurring for different values of $M_{H^\pm}$ in the plots are summarized in Table 3, labeled TC1 to TC7.
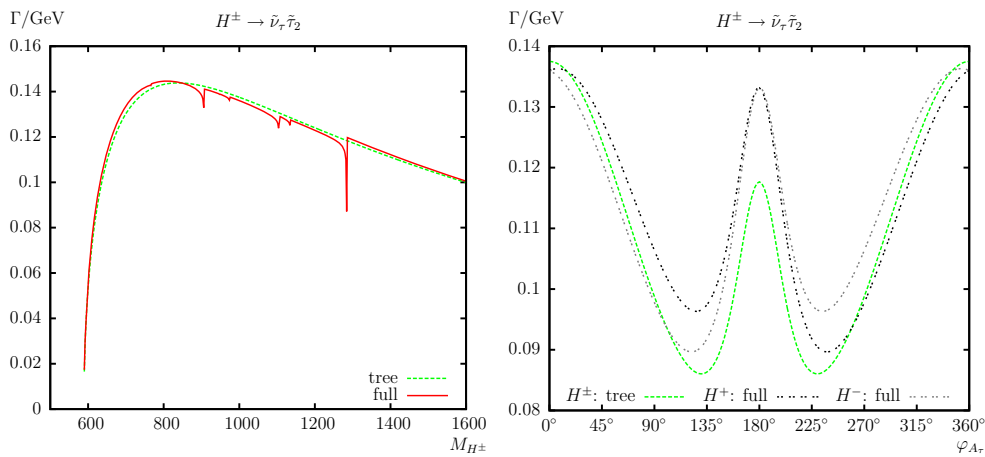
We start with the decay $H^\pm \to \tilde{t}_1 \tilde{b}_1$. In the upper plot of Fig. 3 the dips/thresholds TC3, TC4, TC5, TC6, and TC7 appear; see Table 3. The size of the corrections of the partial decay widths is especially large very close to the production
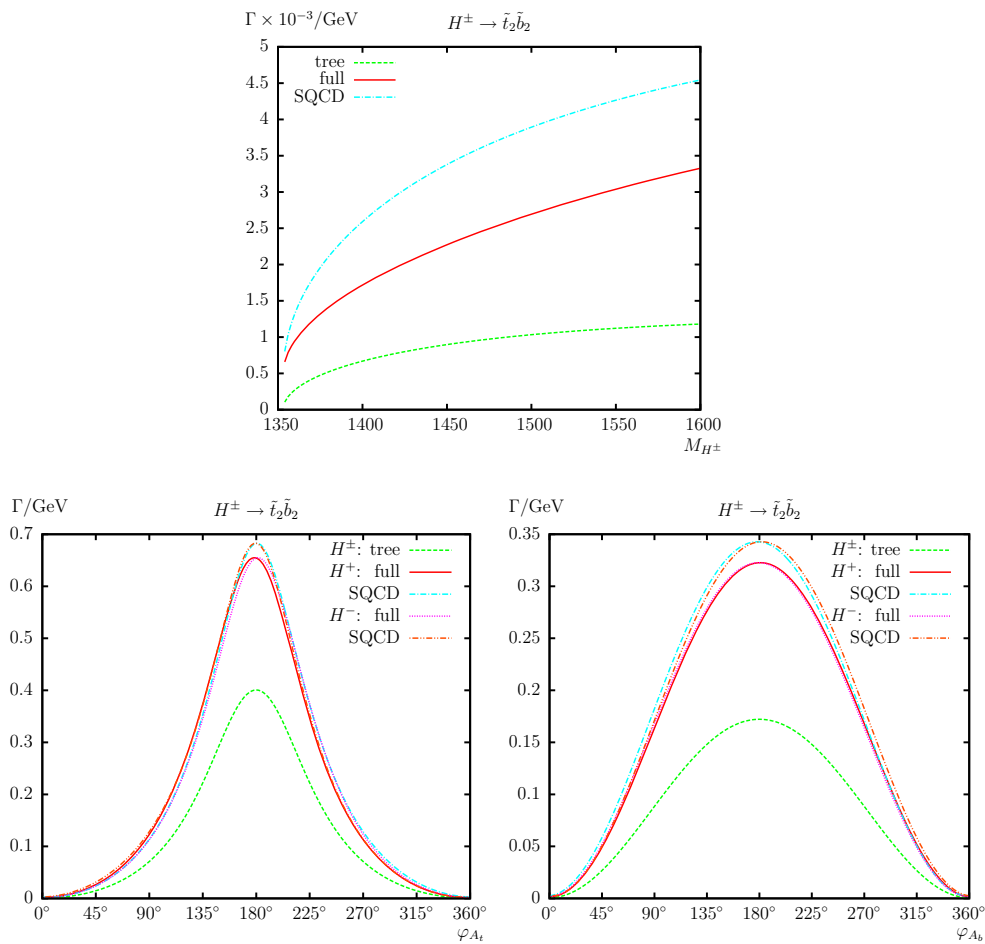
Fig. 6 $\Gamma(H^\pm \to \tilde{t}_2\tilde{b}_2)$. Tree-level, full, and SQCD one-loop corrected partial decay widths are shown. The *upper plot* shows the partial decay width with $M_{H^\pm}$ varied. The *lower plots* show the complex phases φ_{A_t} (*left*) and φ_{A_b} (*right*) varied with parameters chosen according to S2 (see Table 2)
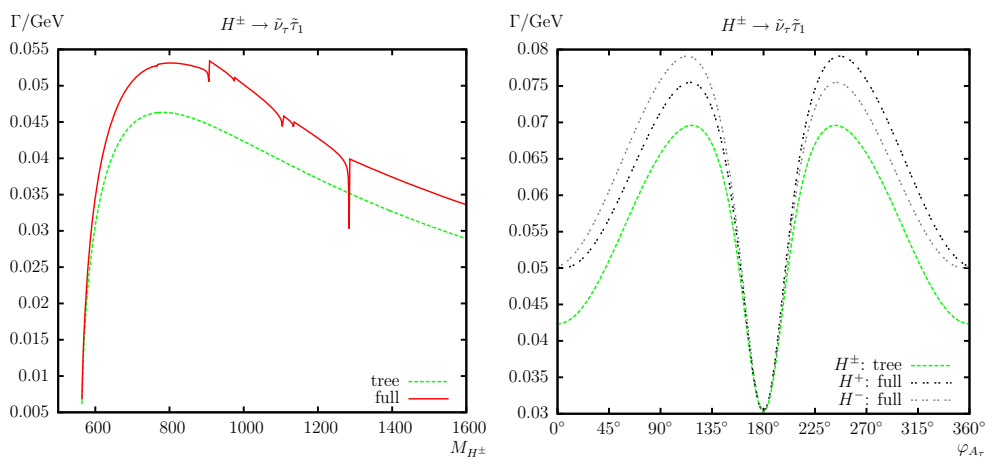
Fig. 7 $\Gamma(H^\pm \to \tilde{\nu}_\tau\tilde{\tau}_1)$. Tree-level and full one-loop corrected partial decay widths are shown. The *left plot* shows the partial decay width with $M_{H^\pm}$ varied; the *right plot* shows the complex phase φ_{A_τ} varied with parameters chosen according to S1 (see Table 2)

Fig. 8 $\Gamma(H^{\pm} \to \tilde{\nu}_{\tau}\tilde{\tau}_2)$. Tree-level and full one-loop corrected partial decay widths are shown. The *left plot* shows the partial decay width with $M_{H^{\pm}}$ varied; the *right plot* shows the complex phase $\varphi_{A_{\tau}}$ varied with parameters chosen according to S1 (see Table 2)

Table 3 Thresholds in charged Higgs-boson decays

TC1:	$M_{H^{\pm}} \approx 768$ GeV	$m_{\tilde{\chi}_1^{\pm}} + m_{\tilde{\chi}_1^0} = M_{H^{\pm}}$
TC2:	$M_{H^{\pm}} \approx 907$ GeV	$m_{\tilde{t}_1} + m_{\tilde{b}_1} = M_{H^{\pm}}$
TC3:	$M_{H^{\pm}} = 976$ GeV	$m_{\tilde{t}_1} + m_{\tilde{b}_2} = M_{H^{\pm}}$
TC4:	$M_{H^{\pm}} \approx 1105$ GeV	$m_{\tilde{\chi}_1^{\pm}} + m_{\tilde{\chi}_4^0} = M_{H^{\pm}}$
TC5:	$M_{H^{\pm}} \approx 1108$ GeV	$m_{\tilde{\chi}_2^{\pm}} + m_{\tilde{\chi}_2^0} = M_{H^{\pm}}$
TC6:	$M_{H^{\pm}} \approx 1135$ GeV	$m_{\tilde{\chi}_2^{\pm}} + m_{\tilde{\chi}_3^0} = M_{H^{\pm}}$
TC7:	$M_{H^{\pm}} \approx 1284$ GeV	$m_{\tilde{t}_2} + m_{\tilde{b}_1} = M_{H^{\pm}}$

threshold[11] from which on the considered decay mode is kinematically possible. Away from this production threshold relative corrections of $\sim +23$ % are found in S1 (see Table 2), of $\sim +5$ % in S2 and of $\sim +3$ % in S3. The SQCD corrections are slightly larger, i.e. the EW corrections reduce the overall size of the loop corrections by ~ 17 %.

In the lower plots of Fig. 3 we show the complex phases $\varphi_{A_{t,b}}$ varied at $M_{H^{\pm}} = 1000$ GeV. The tree-level dependence on the two phases is very different. While for negative A_t a reduction by nearly 50 % w.r.t. positive A_t is found, negative A_b leads to an enhancement of about 25 %. The full corrections with φ_{A_t} varied are up to $\sim +29$ % with slightly larger or lower values for the SQCD corrections by up to $\sim \pm 4$ %. The asymmetry depending on φ_{A_t} is rather small. φ_{A_b} varied can reach $\sim +27$ % with slightly larger values for the SQCD corrections $\sim +31$ %. Here the φ_{A_b} asymmetry is hardly visible.

In Fig. 4 we show the results for $H^{\pm} \to \tilde{t}_1\tilde{b}_2$. In the upper plot the production threshold matches *exactly* $m_{\tilde{t}_1} + m_{\tilde{b}_2} =$

$M_{H^{\pm}} = 976$ GeV. This is due to the fact that all three masses are input parameters (i.e. integers; see Table 2) and our step size for $M_{H^{\pm}}$ is 2 GeV. Therefore the decay width starts "accidentally" exactly from zero. The dips/thresholds appearing are TC4, TC5, TC6, and TC7. Relative corrections of $\sim +8$ % are found at $M_{H^{\pm}} = 1400$ GeV in S2 (see Table 2) (and $\sim +3$ % at $M_{H^{\pm}} = 1600$ GeV in S3). The SQCD corrections alone would lead to an increase of $\sim +21$ % in S2 ($\sim +13$ % in S3), i.e. they overestimate the full corrections by roughly a factor of three.

In the lower plots of Fig. 4 the results are shown for S2 as a function of $\varphi_{A_{t,b}}$. One can see that the size of the corrections to the partial decay width vary substantially with the complex phases $\varphi_{A_{t,b}}$ at $M_{H^{\pm}} = 1400$ GeV. In case of $H^+ \to \tilde{t}_1\tilde{b}_2$ (lower left plot) the behavior in the region $135° < \varphi_{A_t} < 225°$ is due to an accidental interplay of the *shifted* sbottom mixing angle $U_{21}^{\tilde{b}*}$ multiplied with $A_t U_{12}^{\tilde{t}}$, already present in the tree coupling. (In the H^- decay it is complex conjugated: $U_{21}^{\tilde{b}} A_t^* U_{12}^{\tilde{t}*}$.) Furthermore, effects from absorptive contributions also play an important role for the (rather large) asymmetries. The largest contribution to the asymmetries in the lower right plot stems from the $\tilde{t}_1$–$\tilde{b}_2$–γ vertex. At $\varphi_{A_t} = 180°$ the full corrections reach $\sim +23$ %, while the SQCD corrections are much larger $\sim +77$ %. At $\varphi_{A_b} = 90°$ the H^+ (H^-) full corrections reach $\sim +55$ % (~ -22 %), while the SQCD corrections are $\sim +38$ % ($\sim +8$ %).[12]

Next, in Fig. 5 the results for $H^{\pm} \to \tilde{t}_2\tilde{b}_1$ are displayed. In the upper plot the results are shown as a function of $M_{H^{\pm}}$. Relative corrections of $\sim +27$ % are found at

---

[11] It should be noted that a calculation very close to the production threshold requires the inclusion of additional (nonrelativistic) contributions, which is beyond the scope of this paper. Consequently, very close to the production threshold our calculation (at the tree and loop level) does not provide a very accurate description of the decay width.

[12] It should be noted that at $\varphi_{A_b} \approx 180°$ the (*positive*) loop corrections can be larger then the tree results because there the tree-level decay width is accidentally small; see the lower right plot of Fig. 4. In case of large *negative* loop corrections we will add $|\mathcal{M}_{1\text{-loop}}|^2$ to obtain, at least, a positive decay width (see below).
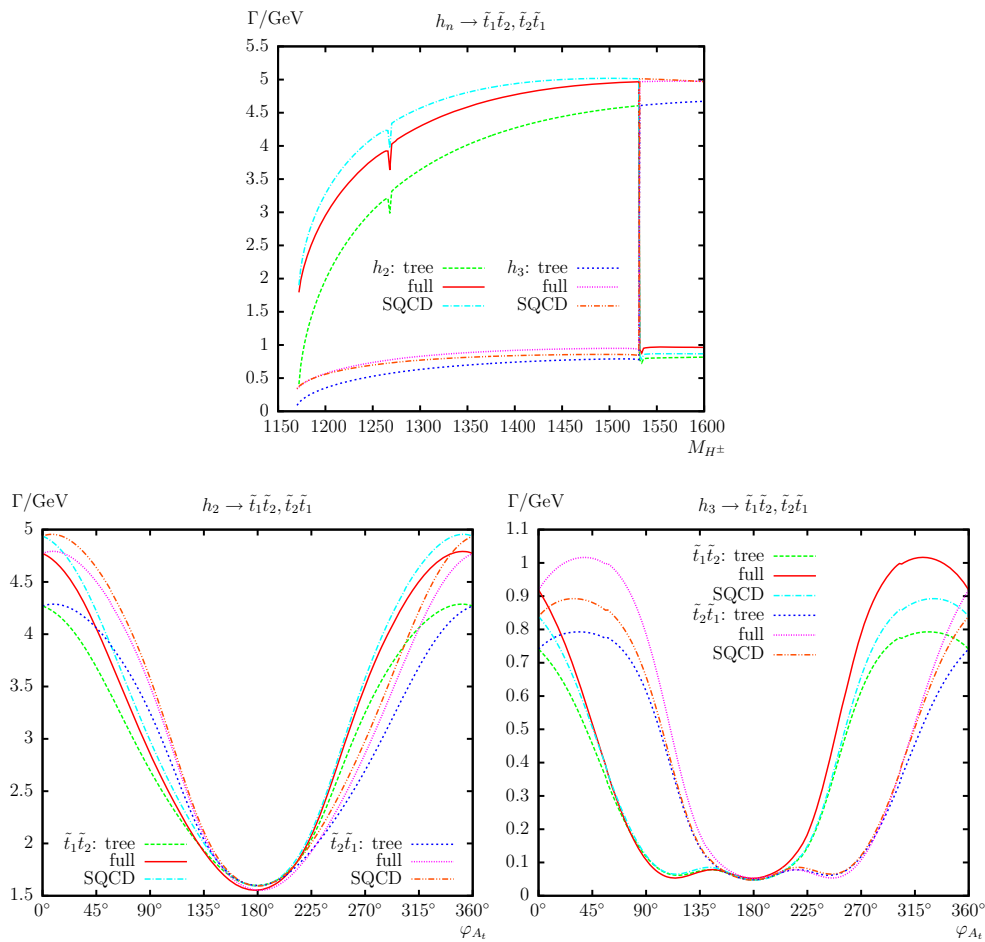
Fig. 9 $\Gamma(h_n \rightarrow \tilde{t}_1\tilde{t}_2, \tilde{t}_2\tilde{t}_1)$. Tree-level, full, and SQCD one-loop corrected partial decay widths are shown. The *upper plot* shows the partial decay width with $M_{H^\pm}$ varied; the *lower plots* show the complex phase φ_{A_t} varied for h_2 decays (*left*) and h_3 decays (*right*) with parameters chosen according to S2 (see Table 2)

$M_{H^\pm} = 1400$ GeV (see Table 2). In this case the EW corrections hardly contribute to the overall one-loop contribution.

In the lower plots the results are displayed as a function of $\varphi_{A_{t,b}}$ in S2. In the left plot one can see that the size of the corrections to the partial decay width vary substantially with the complex phase φ_{A_t}. For all φ_{A_t} the full and SQCD corrections are of similar size and deviate between $+9$ % and $+27$ %. The same holds for φ_{A_b} with small differences between the full and SQCD corrections, which vary only between $+25$ % and $+27$ %. Here the asymmetries are small and hardly visible.

The decay $H^\pm \rightarrow \tilde{t}_2\tilde{b}_2$ is shown in Fig. 6. The overall size of this decay width (with real phases) is (accidentally) very small around $\sim 2 \times 10^{-3}$ GeV. Consequently, the loop corrections, as shown in the upper plot, can be larger than the tree-level result. The SQCD corrections alone would overestimate the full result by about ~ 50 %.

In the lower plots of Fig. 6 one can see that the size of the tree-level result depends again strongly on the two phases. Values of ~ 0.4 (0.16) GeV are reached for negative φ_{A_t} (φ_{A_b}). Again the loop corrections can be substantial. At $\varphi_{A_t} = 180°$ the full corrections reach $\sim +63$ %, while the SQCD corrections are larger $\sim +72$ %. At $\varphi_{A_b} = 180°$ the full corrections reach $\sim +87$ %, while the SQCD corrections are up to $\sim +90$ %. The asymmetries are found to be rather small due to accidentally cancelations with absorptive contributions.

Now we turn to the charged Higgs-boson decays to scalar leptons, $H^\pm \rightarrow \tilde{\nu}_\tau\tilde{\tau}_1$ in Fig. 7 and $H^\pm \rightarrow \tilde{\nu}_\tau\tilde{\tau}_2$ in Fig. 8. The left plots show the results as a function of $M_{H^\pm}$, while the right plots analyze the dependence on φ_{A_τ} for $M_{H^\pm} = 1000$ GeV. In the left plots all seven thresholds, given in Table 3, appear as dips. At $M_{H^\pm} = 1000$ GeV one-loop corrections of $\sim +19$ % are found for $H^\pm \rightarrow \tilde{\nu}_\tau\tilde{\tau}_1$, while for $H^\pm \rightarrow \tilde{\nu}_\tau\tilde{\tau}_2$ they are only ~ -1 %.

The maximum values of the full one-loop corrections as a function of φ_{A_τ} reach $\sim +15$ % ($+13$ %) for $H^\pm \rightarrow \tilde{\nu}_\tau\tilde{\tau}_1(\tilde{\nu}_\tau\tilde{\tau}_2)$. The asymmetries in the decays of a negative
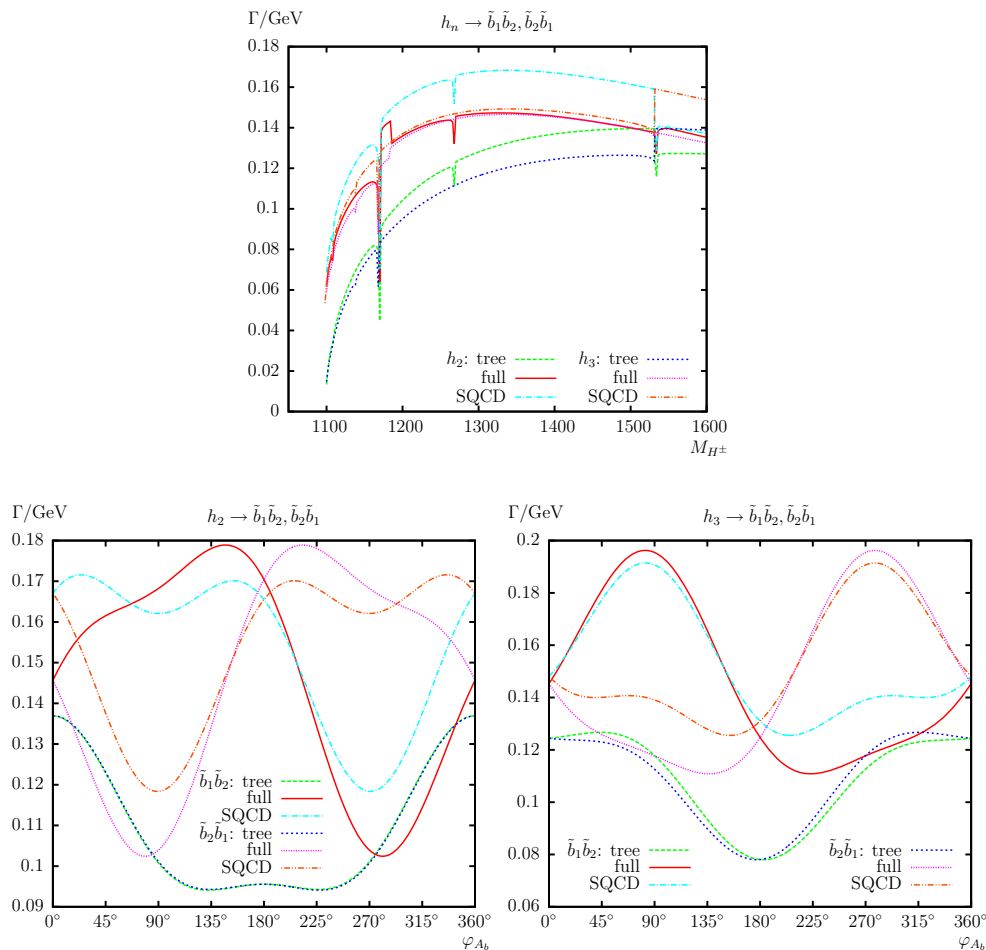
Fig. 10 $\Gamma(h_n \to \tilde{b}_1\tilde{b}_2, \tilde{b}_2\tilde{b}_1)$. Tree-level, full, and SQCD one-loop corrected partial decay widths are shown. The *upper plot* shows the partial decay width with $M_{H^\pm}$ varied; the *lower plots* show the com-
plex phase φ_{A_b} varied for h_2 decays (*left*) and h_3 decays (*right*) with parameters chosen according to S2 (see Table 2)

charged Higgs w.r.t. a positively charged Higgs are substantial. The size of the respective loop corrections can nearly be twice as large in one case w.r.t. to the other, depending whether $\varphi_{A_\tau} \leq 180°$ or $\varphi_{A_\tau} \geq 180°$ is considered.

4.3.2 h_n decays into sfermions

We now turn to the decay modes $h_n \to \tilde{f}_i \tilde{f}_j$ ($n = 2, 3; i, j = 1, 2$). Results are shown in the Figs. 9, 10, 11, 12, 13, 14, 15, 16, 17 and 18.

Before discussing every figure in detail, it should be noted that there is a subtleness concerning the mixture of the h_n bosons. Depending on the input parameters, the higher-order corrections to the three neutral Higgs-boson masses can vary substantially. The mass ordering $m_{h_1} < m_{h_2} < m_{h_3}$ (as performed automatically by FeynHiggs), even in the case of real parameters, can yield a heavy $\mathcal{CP}$-even Higgs mass higher *or* lower than the (heavy) $\mathcal{CP}$-odd Higgs mass. Such a

transition in the mass ordering (or "mass crossing") is accompanied by an abrupt change in the Higgs mixing matrix $\hat{\mathbf{Z}}$.[13] For our input parameters (see Table 2) there are two (possible) crossings. The first (called "MC1" below) appears at $M_{H^\pm} \approx 1006$ GeV. Before the crossing we find $h_2 \sim H$ ($h_3 \sim A$), whereas after the crossing it changes to $h_2 \sim A$ ($h_3 \sim H$). The second crossing (called "MC2") is found at $M_{H^\pm} \approx 1532$ GeV, i.e. the changing of the mixture from $h_2 \sim A$ ($h_3 \sim H$) to $h_2 \sim H$ ($h_3 \sim A$). Very close to the mass crossings the $\hat{\mathbf{Z}}$ matrix can yield small numerical instabilities. As an example, for 1532 GeV $\lesssim M_{H^\pm} \lesssim$ 1536 GeV the $\hat{\mathbf{Z}}$ matrix causes structures appearing similar to "usual" dips from thresholds. All the dips/thresholds (some are hardly

---

[13] In our case the Z-factor matrix $\hat{Z}_{ij} \equiv$ ZHiggs[i, j]; see Ref. [57] (and Ref. [33]), which contributes at tree level. Furthermore, $\hat{\mathbf{Z}}$ is calculated by FeynHiggs, which uses $m_b(m_b)$ and tree-level sfermion masses instead of the shifted masses, causing a slight displacement in the threshold position.
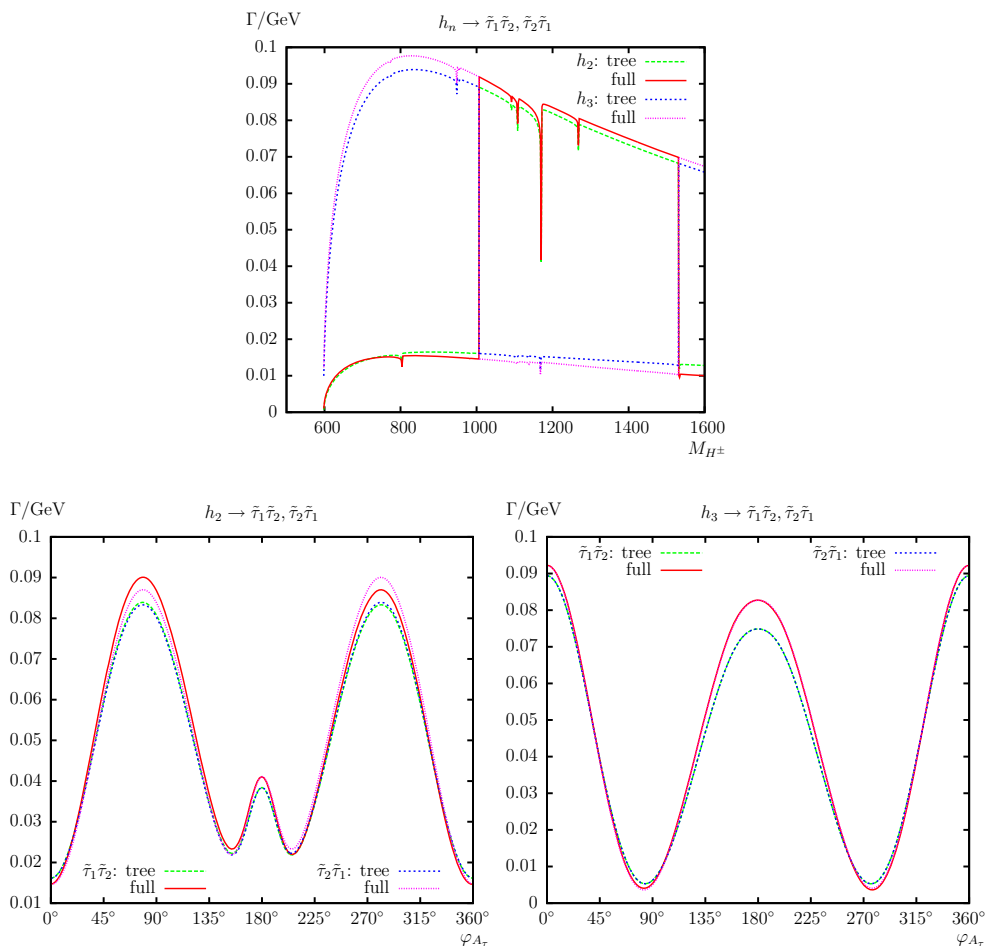
Fig. 11 $\Gamma(h_n \to \tilde{\tau}_1\tilde{\tau}_2, \tilde{\tau}_2\tilde{\tau}_1)$. Tree-level and full one-loop corrected partial decay widths are shown. The *upper plot* shows the partial decay width w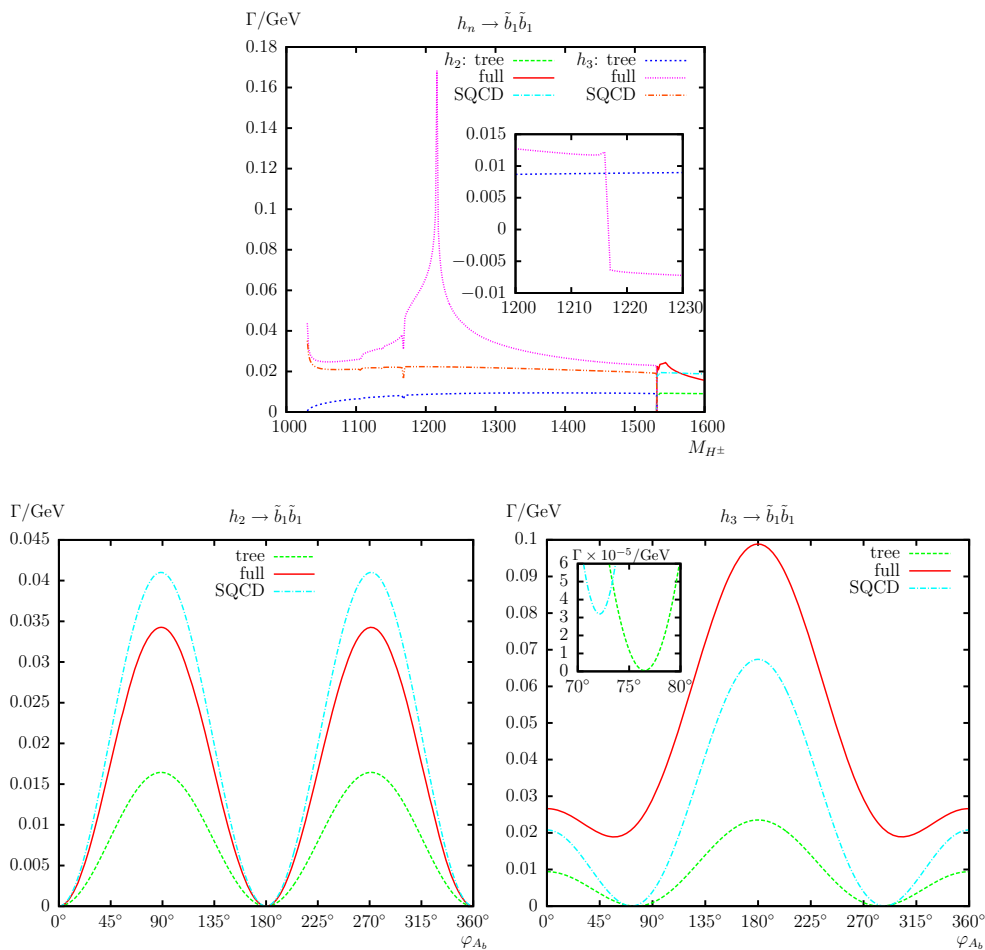ith $M_{H^\pm}$ varied; the *lower plots* show the complex phase φ_{A_τ} varied for h_2 decays (*left*) and h_3 decays (*right*) with parameters chosen according to S1 (see Table 2)

visible) appearing in the figures are listed in Table 4, labeled as TN1 to TN17.

We start with the decay $h_n \to \tilde{t}_1\tilde{t}_2, \tilde{t}_2\tilde{t}_1$ as shown in Fig. 9. The upper plot shows the results as a function of $M_{H^\pm}$, whereas in the lower plots we present the decay widths as a function of φ_{A_t} in S2. We show separately the results for the h_2 and h_3 decay widths. In the upper plot of Fig. 9 the dips/thresholds TN16 and TN17 appear. Away from the production threshold relative corrections of $\sim +12$ % are found in S2 (see Table 2) for the h_2 decay. There the SQCD corrections overestimate the full correction by about 30 %. In case of the h_3 decay the relative corrections are $\sim +24$ % in S2 (see Table 2) and the SQCD corrections underestimate the full result by about 50 %. The MC2 can be observed at $M_{H^\pm} \sim 1532$ GeV as described above. Here h_2 and h_3 change their role. Within the unrotated scalar top basis the $\mathcal{CP}$-odd Higgs boson can only decay as $A \to \tilde{t}_L\tilde{t}_R, \tilde{t}_R\tilde{t}_L$, but not as $A \to \tilde{t}_L\tilde{t}_L, \tilde{t}_R\tilde{t}_R$, whereas the $\mathcal{CP}$-even Higgs boson has all four decays possible. Consequently, the decay to $\tilde{t}_1\tilde{t}_2, \tilde{t}_2\tilde{t}_1$ can depend strongly on the $\mathcal{CP}$ nature of the decaying Higgs boson. While below MC2 we find $\Gamma(h_2 \to \tilde{t}_1\tilde{t}_2, \tilde{t}_2\tilde{t}_1) \gg \Gamma(h_3 \to \tilde{t}_1\tilde{t}_2, \tilde{t}_2\tilde{t}_1)$, above MC2 we have correspondingly $\Gamma(h_2 \to \tilde{t}_1\tilde{t}_2, \tilde{t}_2\tilde{t}_1) \ll \Gamma(h_3 \to \tilde{t}_1\tilde{t}_2, \tilde{t}_2\tilde{t}_1)$, as can be clearly observed in the upper plot of Fig. 9.

We now turn to the phase dependence of the decay width shown in S2, i.e. for $M_{H^\pm} = 1400$ GeV, where the left (right) plot in Fig. 9 shows the dependence of $\Gamma(h_2 \to \tilde{t}_1\tilde{t}_2, \tilde{t}_2\tilde{t}_1)$ $(\Gamma(h_3 \to \tilde{t}_1\tilde{t}_2, \tilde{t}_2\tilde{t}_1))$ on φ_{A_t}. In the lower left plot one can observe that already the tree-level result (green dashed) and the tree of the conjugated process (blue short dashed) are asymmetric and depend strongly on the phase. The asymmetry at the tree level is due to the contribution from the $\hat{\mathbf{Z}}$ matrix, which is not in general unitary and depends via the stop contributions to the Higgs boson self-energies on φ_{A_t}; see Ref. [33]. While for $\varphi_{A_t} \sim 180°$ a width of about 1.5 GeV is observed, for $\varphi_{A_t} \sim 0°$ a three times higher decay width is found. The full corrections for φ_{A_t} varied are $\lesssim +12$ % for S2, while the SQCD corrections overestimate the full corrections up to 30 %. In the lower right plot of Fig. 9, where we show the φ_{A_t} dependence of the h_3 decay one can see that as

Fig. 12 $\Gamma(h_n \rightarrow \tilde{b}_1\tilde{b}_1)$. Tree-level, full, and SQCD one-loop corrected partial decay widths are shown. The *upper plot* shows the partial decay width wi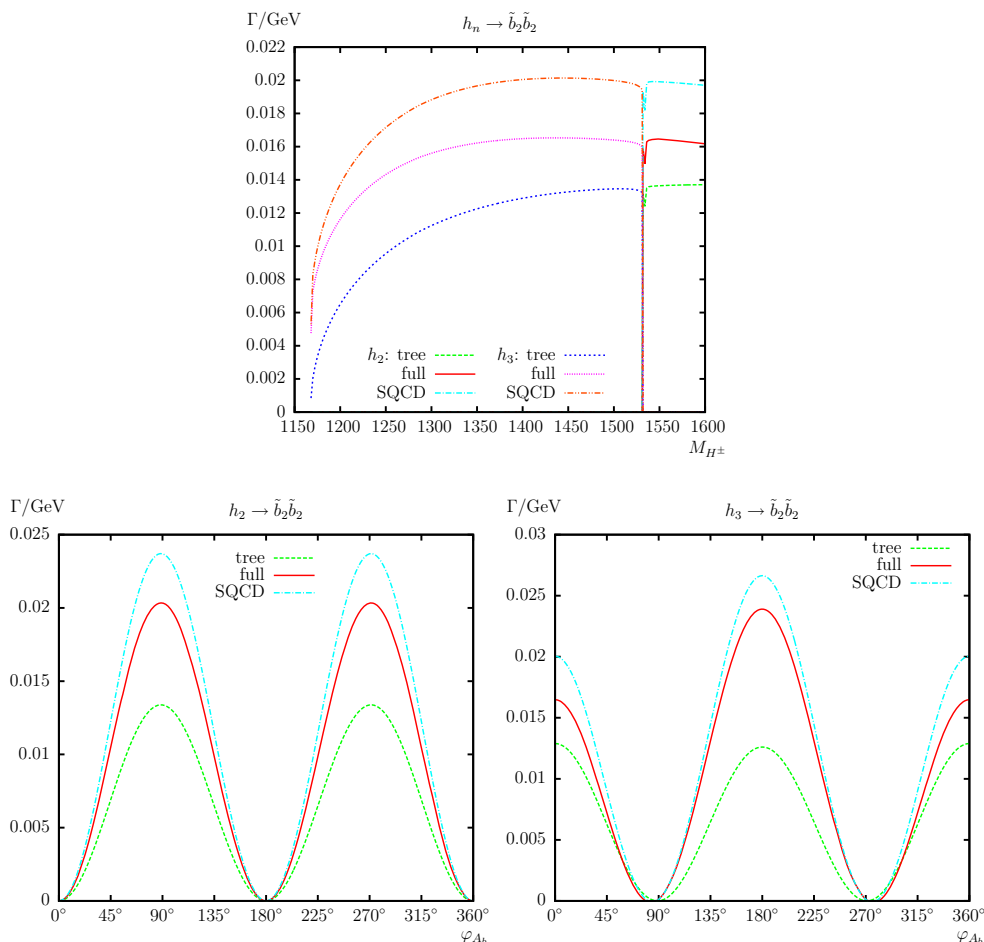th $M_{H^\pm}$ varied; the *lower plots* show the complex phase φ_{A_b} varied for h_2 decays (*left*) and h_3 decays (*right*) with parameters chosen according to S2 (see Table 2)

for the h_2 case already the tree-level results (green dashed) and the tree of the conjugated process (blue short dashed) depend strongly on the phase and exhibit an asymmetry. The latter is again due to the contribution from the $\hat{\mathbf{Z}}$ matrix. The relative corrections for φ_{A_t} are up to ∼+29 % for S2. The SQCD corrections are smaller and would underestimate the full corrections by more than 50 %.

In Fig. 10 we present the results for the decays $h_n \rightarrow \tilde{b}_1\tilde{b}_2, \tilde{b}_2\tilde{b}_1$, where in the upper (lower) row we show the dependence on $M_{H^\pm}$ (φ_{A_b}). In the upper row plot the dips/thresholds TN11, TN12, TN15, TN16, and TN17 appear. The step at $M_{H^\pm} \approx 1184$ GeV is an anomalous threshold (see p. 376 in Ref. [115]) and could be traced back to the C-functions $C_{0,1,2}(m_{h_2}^2, m_{\tilde{b}_1}^2, m_{\tilde{b}_2}^2, m_{\tilde{t}_i}^2, m_{\tilde{t}_j}^2, M_W^2)$ with $i \neq j$. The parameter regions very close to these steps are expected to be somewhat unreliable and should be interpreted with care. At $M_{H^\pm} = 1400$ GeV the full one-loop corrections to the h_2 decay reach only ∼+6 %, while the SQCD corrections would overestimate this by a factor of ∼2.5. Now we turn to the corresponding h_3 decay. The first three dips and the

step at $M_{H^\pm} \approx 1182$ GeV are the same as for the h_2 decay; see above. For the decay of the h_3 at $M_{H^\pm} = 1400$ GeV we find full corrections at the level of +17 %, where the SQCD results are only slightly larger. As in Fig. 9 one can observe the MC2 with an "interchange" of h_2 and h_3.

In the lower left plot of Fig. 10 we present $\Gamma(h_2 \rightarrow \tilde{b}_1\tilde{b}_2, \tilde{b}_2\tilde{b}_1)$ as a function of φ_{A_b} in S2. The variation with φ_{A_b} is found to be very large, full relative corrections are up to ∼+90 % for S2, where the SQCD corrections account for about 60 % of those. This can partially be attributed to the very small tree level within the region $60° \lesssim \varphi_{A_b} \lesssim 300°$. Furthermore, a very strong asymmetry between one decay and its complex conjugate can be observed, reaching up to 60 %. In the lower right plot the corresponding results for the h_3 decay are shown. One can see that again already the tree-level result (green dashed) and the tree of the conjugated process (blue short dashed) are asymmetric, which is caused again by the $\hat{\mathbf{Z}}$ matrix contribution, where φ_{A_b} enters via the $\tilde{b}$ contributions to the Higgs-boson self-energies. As in the h_2 case the size of the corrections shows also a large variation

Fig. 13 $\Gamma(h_n \rightarrow \tilde{b}_2 \tilde{b}_2)$. Tree-level, full, and SQCD one-loop corrected partial decay widths are shown. The *upper plot* shows the partial decay width with $M_{H^\pm}$ varied; the *lower plots* show the complex phase φ_{A_b} varied for h_2 decays (*left*) and h_3 decays (*right*) with parameters chosen according to S2 (see Table 2)

with φ_{A_b}. The full relative corrections are up to $\sim +66\%$ for S2, where the SQCD corrections are only slightly smaller.

The third "mixed case", the decays $h_n \rightarrow \tilde{\tau}_1 \tilde{\tau}_2, \tilde{\tau}_2 \tilde{\tau}_1$, is shown in Fig. 11. As before, the upper plots depict the result as a function of $M_{H^\pm}$, whereas the lower row presents the φ_{A_τ} dependence. Here it should be noted that in many MSSM scenarios (as in the numerical example chosen here) the scalar taus are lighter than the scalar quarks. Consequently, even a small decay width could result in a relatively large BR. We start our numerical description with the h_2 decay as a function of $M_{H^\pm}$. The first dip is the threshold TN5; see Table 4. The second (small) dip is the threshold TN9.[14] Furthermore, the dips/thresholds TN11, TN12, TN15, TN16, and TN17 appear. At $M_{H^\pm} = 1000$ GeV the full one-loop corrections

reach $\sim -9\%$. In the same plot we show also the results for the h_3 decay. Here the dips/thresholds TN3, TN6, TN7, TN10, TN13, and TN14 appear. At $M_{H^\pm} = 1000$ GeV the full one-loop corrections reach $\sim +3\%$. The two mass crossings, MC1 and MC2, can again be observed, where h_2 and h_3 interchange their $\mathcal{CP}$ character.

We now turn to the results for the h_2 (h_3) decay as a function of φ_{A_τ} in the lower left (right) plot of Fig. 11. For the h_2 decay the relative corrections for $\varphi_{A_\tau} = 80°, 180°, 280°$ are up to $\sim +7\%$ in S1. For the h_3 decay, on the other hand, the relative corrections for $\varphi_{A_\tau} = 82°, 180°$ are up to $\sim -24\%, \sim +10\%$ in S1. The asymmetry is too small to be visible in the plot.

Next we consider h_n decays into sfermions with equal sfermion indices and it should be noted that the $A\tilde{f}_i \tilde{f}_i$ ($i = 1, 2$) couplings are exactly zero in case of real input parameters.

In Fig. 12 we present the results for the decays $h_n \rightarrow \tilde{b}_1 \tilde{b}_1$. The dependence on $M_{H^\pm}$ is shown in the upper plot, whereas the dependence on φ_{A_b} for $M_{H^\pm} = 1400$ GeV is given in the

---

[14] It should be noted that the "squark" thresholds (in a h_n decay into sleptons) enter *into the tree level* only via the $\hat{\mathbf{Z}}$ matrix contribution. Via $2\mathrm{Re}\{\mathcal{M}^*_{\mathrm{tree}} \mathcal{M}_{\text{1-loop}}\}$ these effects propagate also into the loop corrections. (Of course there are in addition pure loop corrections from the squark–squark–slepton–slepton couplings; see third row, third column of Fig. 1.)
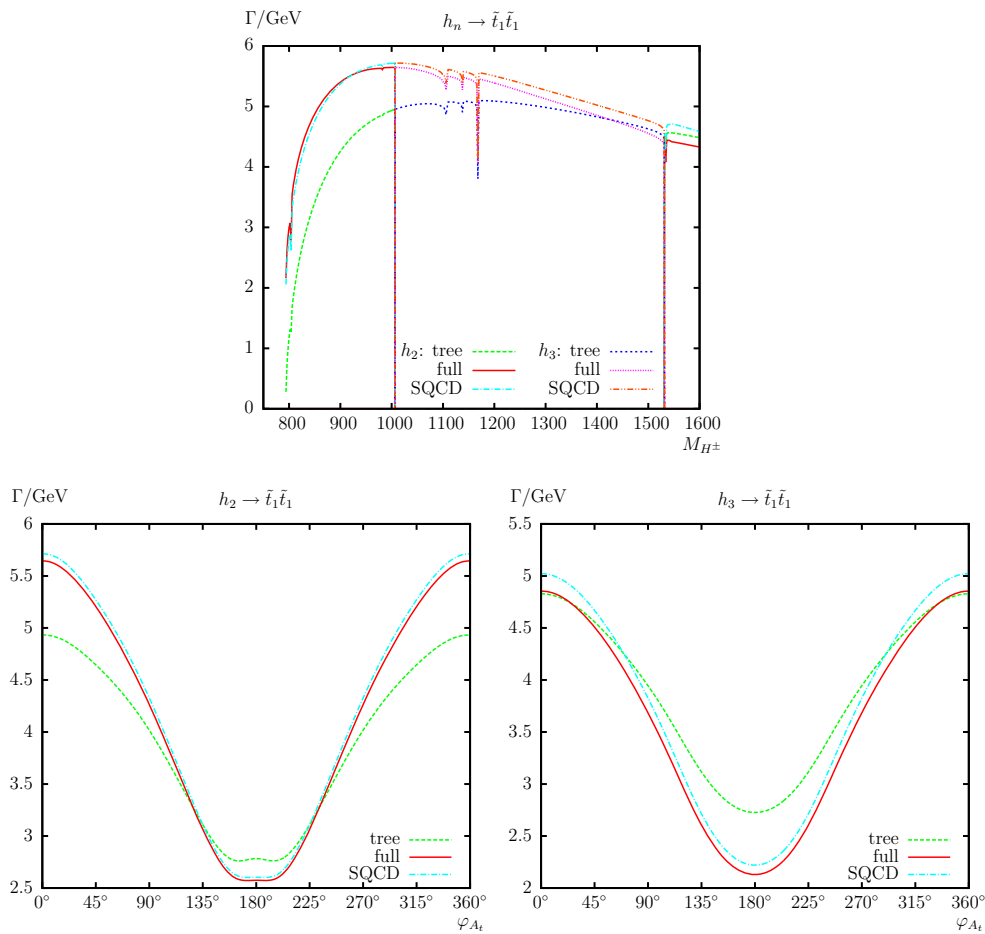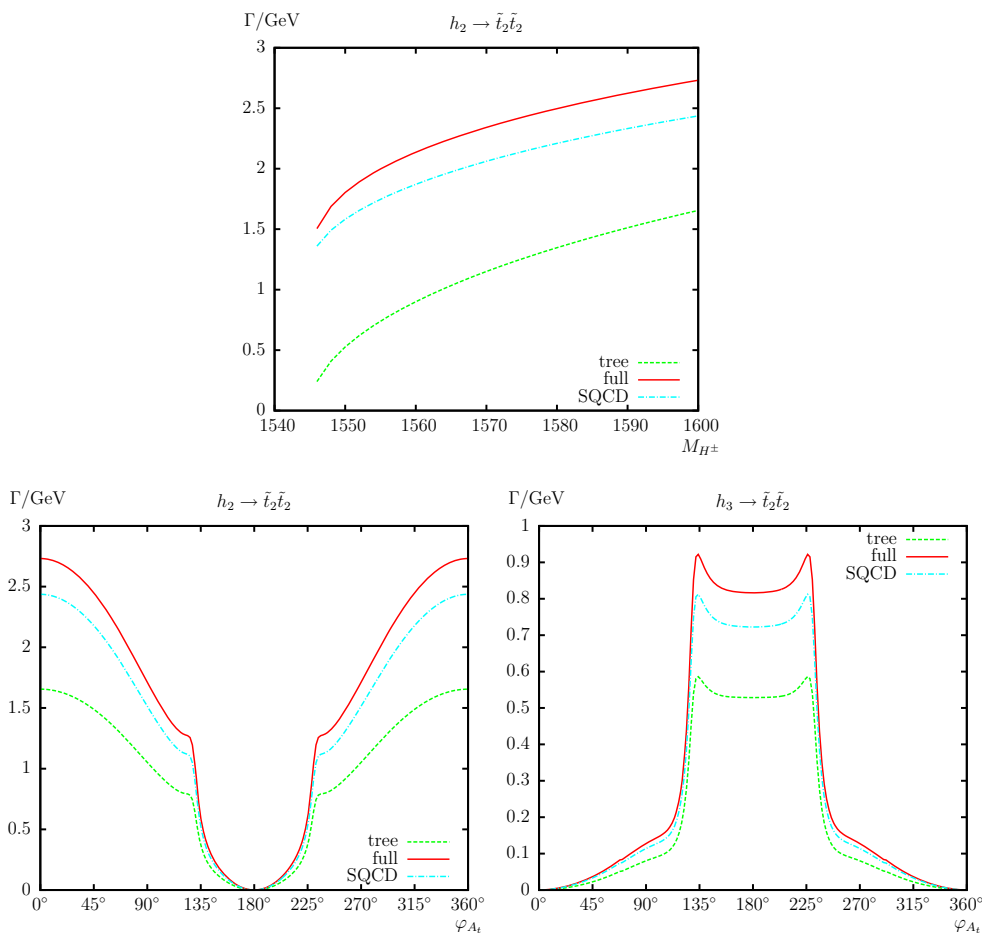
Fig. 14 $\Gamma(h_n \to \tilde{t}_1 \tilde{t}_1)$. Tree-level, full, and SQCD one-loop corrected partial decay widths are shown. The *upper plot* shows the partial decay width with $M_{H^\pm}$ varied; the *lower plots* show the complex phase φ_{A_b} varied for h_2 decays (*left*, S1) and h_3 decays (*right*, S2)

lower plots. We start with $\Gamma(h_2 \to \tilde{b}_1 \tilde{b}_1)$ in the upper plot. Only above MC2 this decay width becomes non-zero. The peak at $M_{H^\pm} \approx 1545$ GeV (red line) is the threshold TN18. Furthermore, the tree-level decay width $\Gamma(h_2 \to \tilde{b}_1 \tilde{b}_1)$ is accidentally very small for the parameter set chosen; see Table 2. Because of this smallness, the relative size of the one-loop correction becomes larger than the tree level, and it can even turn negative. Therefore, in this case (i.e. negative decay width) we added $|\mathcal{M}_{1\text{-loop}}|^2$ to the full one-loop result to obtain a positive decay width. The full relative corrections are $\sim+73$ % at $M_{H^\pm} = 1600$ GeV and the SQCD corrections are $\sim+80$ %. Also shown in this plot is the decay $h_3 \to \tilde{b}_1 \tilde{b}_1$, which is non-zero below MC2. For this decay the dips/thresholds TN10, TN13, and TN14 appear. The large "spike" at $M_{H^\pm} \approx 1216$ GeV is caused by the addition of the two-loop contribution $|\mathcal{M}_{1\text{-loop}}|^2$ as explained above (formally it is caused by the anomalous thresholds of the C-functions $C_{0,1,2}(m_{h_3}^2, m_{\tilde{b}_1}^2, m_{\tilde{b}_1}^2, m_{\tilde{t}_i}^2, m_{\tilde{t}_j}^2, M_W^2)$ with $i \neq j$). Without the two-loop contribution it appears as step (see the inlay in the upper plot of Fig. 12) similar to Fig. 10. Because of the smallness of the tree, the full relative corrections reach

$\sim+183$ % at $M_{H^\pm} = 1400$ GeV. Here the SQCD corrections are smaller with $\sim+92$ %.

In the lower left plot of Fig. 12 we show the h_2 decay with the complex phase φ_{A_b} varied at $M_{H^\pm} = 1400$ GeV. For $\varphi_{A_b} = 0°, 180°, 360°$, i.e. real parameters the h_2 decay is purely $\mathcal{CP}$-odd, and thus the decay width is zero. For complex values of the phase small, but non-zero values are reached. Here, for the same reasons as in the upper plot the loop corrections can be larger than the tree level and reach actually $\sim+108$ % (and $\sim+125$ % for SQCD) at $\varphi_{A_b} = 90°, 270°$. In the lower right plot of Fig. 12 we show the h_3 decay with the complex phase φ_{A_b} varied at $M_{H^\pm} = 1400$ GeV. Here (for the same reasons as in the upper plot) the loop corrections can be larger then the tree level (and for consistency with the upper plot we also added $|\mathcal{M}_{1\text{-loop}}|^2$ here) and reach up to $\sim+320$ % (and $\sim+165$ % for SQCD) at $\varphi_{A_b} = 180°$. It should be noted that the SQCD decay width at $\varphi_{A_b} \approx 76°, 284°$ does *not* go to zero due to $|\mathcal{M}_{1\text{-loop}}|^2$, but just reaches a (very) small value of $\Gamma(h_3 \to \tilde{b}_1 \tilde{b}_1)$ (see the inlay in the lower right plot of Fig. 12). For S2 we have $h_3 \sim H$ and the $\hat{\mathbf{Z}}$ matrix depends rather weak on A_b, i.e.

Fig. 15 $\Gamma(h_n \to \tilde{t}_2\tilde{t}_2)$. Tree-level, full, and SQCD one-loop corrected partial decay widths are shown. The *upper plot* shows the partial decay width with $M_{H^\pm}$ varied; the *lower plots* show the complex phase φ_{A_t} varied for h_2 decays (*left*) and h_3 decays (*right*) with parameters chosen according to S3 (see Table 2)

the main effect on the decay width stems *continuously* from the $\hat{Z}$ matrix element $\hat{Z}_{32}$. In contrast to the left plot the tree decay width is zero at $\varphi_{A_b} \approx 76°, 284°$, because the relevant $(\propto \hat{Z}_{32})$ real part of the coupling $C(h_3, \tilde{b}_1, \tilde{b}_1)$, see Ref. [87], accidentally goes through zero.

In Fig. 13 we present the decay $h_n \to \tilde{b}_2\tilde{b}_2$, in full analogy to Fig. 12. The same behavior of h_2 and h_3 concerning MC2 can be observed. The full relative corrections for the h_2 decay are $\sim+18$ % at $M_{H^\pm} = 1600$ GeV, where the pure SQCD corrections would overestimate this correction by a factor ~1.8. The decay $h_3 \to \tilde{b}_2\tilde{b}_2$ is again non-zero only below MC2. The dip (hardly visible at $M_{H^\pm} \approx 1168$ GeV) in the h_3 decay is the threshold TN14. The full relative corrections are $\sim+28$ % at $M_{H^\pm} = 1400$ GeV and the SQCD corrections are larger by about a factor of 1.6.

In the lower left plot of Fig. 13 we show the variation of $\Gamma(h_2 \to \tilde{b}_2\tilde{b}_2)$ with φ_{A_b} at $M_{H^\pm} = 1400$ GeV. Here the loop corrections reach $\sim+52$ % (and $\sim+60$ % for SQCD) at $\varphi_{A_b} = 90°, 270°$. The decay width goes to zero for real A_b due to the $\mathcal{CP}$-nature of the h_2. In the lower right plot of Fig. 13 we show $\Gamma(h_3 \to \tilde{b}_2\tilde{b}_2)$ with φ_{A_b} var-

ied at $M_{H^\pm} = 1400$ GeV. Here the loop corrections reach $\sim+90$ % at $\varphi_{A_b} = 180°$ and are slightly overestimated in the pure SQCD case. The tree decay width goes to zero for $\varphi_{A_b} \approx 85°, 275°$, for the same reasons as discussed above for Fig. 12. We have again $h_3 \sim H$, i.e. the main effect on the decay width stems from $\hat{Z}_{32}$.

We now turn to the neutral Higgs decay to scalar top quarks, which are shown in full analogy to the decay to scalar bottom quarks above. In Fig. 14 we present the decay $h_n \to \tilde{t}_1\tilde{t}_1$. In the upper row we show the results as a function of $M_{H^\pm}$. The dips/thresholds appearing in the h_2 decay are TN5 and TN8. The full relative corrections are $\sim+14$ % at $M_{H^\pm} = 1000$ GeV (i.e. S1) and the SQCD corrections are $\sim+16$ %. The decay width turns zero between MC1 and MC2 and reaches non-zero values below MC1 and above MC2. Reversely, we find non-zero values for $\Gamma(h_3 \to \tilde{t}_1\tilde{t}_1)$ only between MC1 and MC2. The dips in the h_3 decay are the thresholds TN10, TN13, and TN14. The full relative corrections at $M_{H^\pm} = 1400$ GeV are accidentally small and reach only +1 %, where the pure SQCD corrections reach $\sim+4$ %.
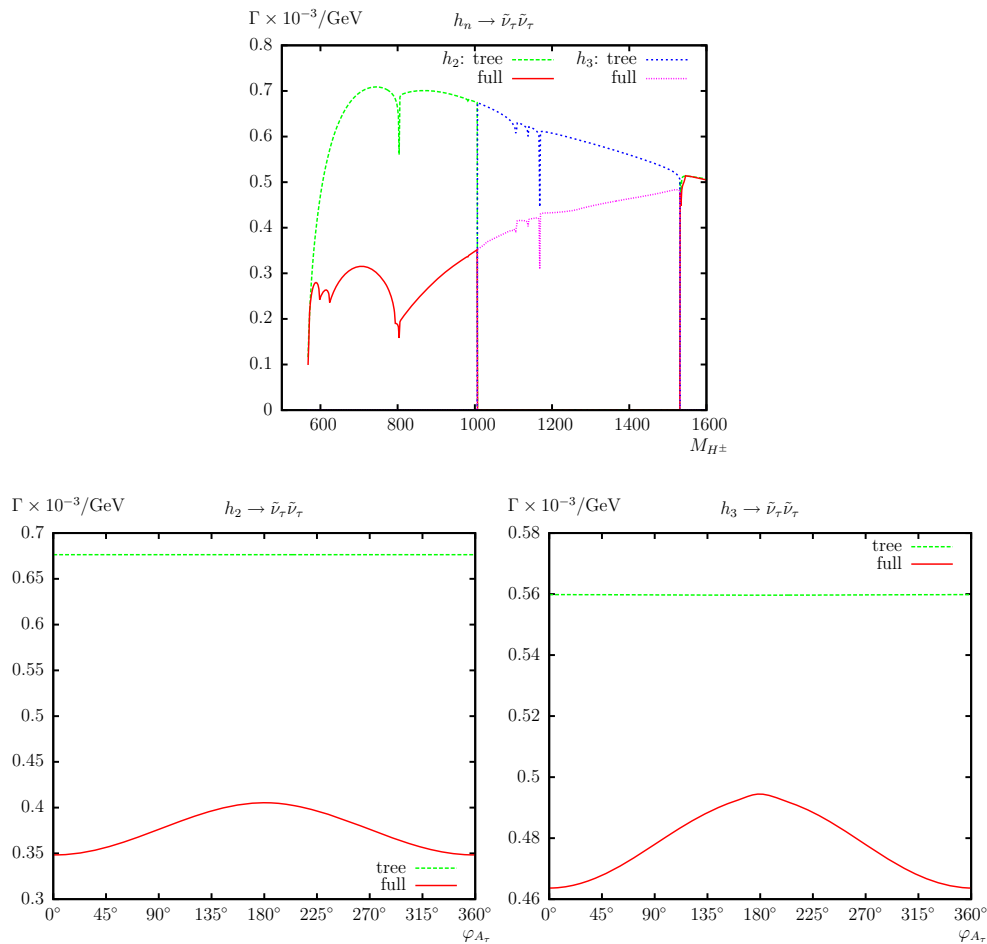
Fig. 16 $\Gamma(h_n \to \tilde{\nu}_\tau \tilde{\nu}_\tau)$. Tree-level and full one-loop corrected partial decay widths are shown. The *upper plot* shows the partial decay width with $M_{H^\pm}$ varied; *the lower plots* show the complex phase φ_{A_τ} varied for h_2 decays (*left*, S1) and h_3 decays (*right*, S2)

In the lower left plot of Fig. 14 we show the h_2 decay with the complex phase φ_{A_t} varied at $M_{H^\pm} = 1000$ GeV. Here the loop corrections can vary between $\sim +14\%$ for $\varphi_{A_t} \sim 0°, 360°$ and $\sim -7\%$ at $\varphi_{A_t} = 180°$, where the SQCD corrections in this case are a good approximation to the full result. In the lower right plot of Fig. 14 we show the h_3 decay with φ_{A_t} varied at $M_{H^\pm} = 1400$ GeV. Here the loop corrections are close to zero for real positive values of A_b, where the EW corrections compensate the SQCD contributions. The full corrections can reach $\sim -22\%$ (and $\sim -19\%$ for SQCD) at $\varphi_{A_t} = 180°$.

The final decays involving stops are shown in Fig. 15. The results as a function of $M_{H^\pm}$ are given in the upper plot. Due to the large values of $m_{\tilde{t}_2}$ for real parameters only $\Gamma(h_2 \to \tilde{t}_2\tilde{t}_2)$ reaches non-zero values, because $h_2 \sim H$ and $h_3 \sim A$. The full relative corrections for the h_2 decay are $\sim +65\%$ at $M_{H^\pm} = 1600$ GeV (i.e. S3) and the SQCD corrections reach $\sim +47\%$.

In the lower left plot of Fig. 15 we show $\Gamma(h_2 \to \tilde{t}_2\tilde{t}_2)$ with the complex phase φ_{A_t} varied at $M_{H^\pm} = 1600$ GeV. The smooth structure around $\varphi_{A_t} = 130°, 230°$ is *not* a threshold

but an interplay of $\hat{Z}_{22}$ multiplied by the corresponding (real and imaginary) part of the coupling $C(h_2, \tilde{t}_2, \tilde{t}_2)$; see Ref. [87]. For $\varphi_{A_t} = 180°$ the decay width goes to zero, since there is an evolving mass crossing from $\varphi_{A_t} = 0°$ ($h_2 \sim H$) to $\varphi_{A_t} = 180°$ ($h_2 \sim A$) due to the strong dependence of the $\hat{Z}$ matrix from A_t, i.e. a strong variation with φ_{A_t}. The loop corrections can reach $\sim +63\%$ (and $\sim +44\%$ for SQCD) at $\varphi_{A_t} = 90°, 270°$. The h_3 decay is non-zero above MC2 only for complex parameters. In the lower right plot of Fig. 15 we show $\Gamma(h_3 \to \tilde{t}_2\tilde{t}_2)$ with φ_{A_t} varied at $M_{H^\pm} = 1600$ GeV. The smooth structure around $\varphi_{A_t} = 135°, 225°$ is mainly a numerical effect of the $\hat{Z}$ matrix element $\hat{Z}_{33}$. The loop corrections can reach $\sim +54\%$ (and $\sim +37\%$ for SQCD) at $\varphi_{A_t} = 180°$.

We finish our numerical analysis with the remaining decays to scalar leptons. In Fig. 16 the decay widths for $h_n \to \tilde{\nu}_\tau \tilde{\nu}_\tau$ are shown. In the upper plot the results as a function of $M_{H^\pm}$ are given. The decay $h_2 \to \tilde{\nu}_\tau \tilde{\nu}_\tau$ for real parameters is non-zero below MC1 and above MC2 due to the $\mathcal{CP}$-structure of h_2. The dips/thresholds appearing for the h_2 decay are TN1, TN2, TN4, TN5, and TN8. The full relative
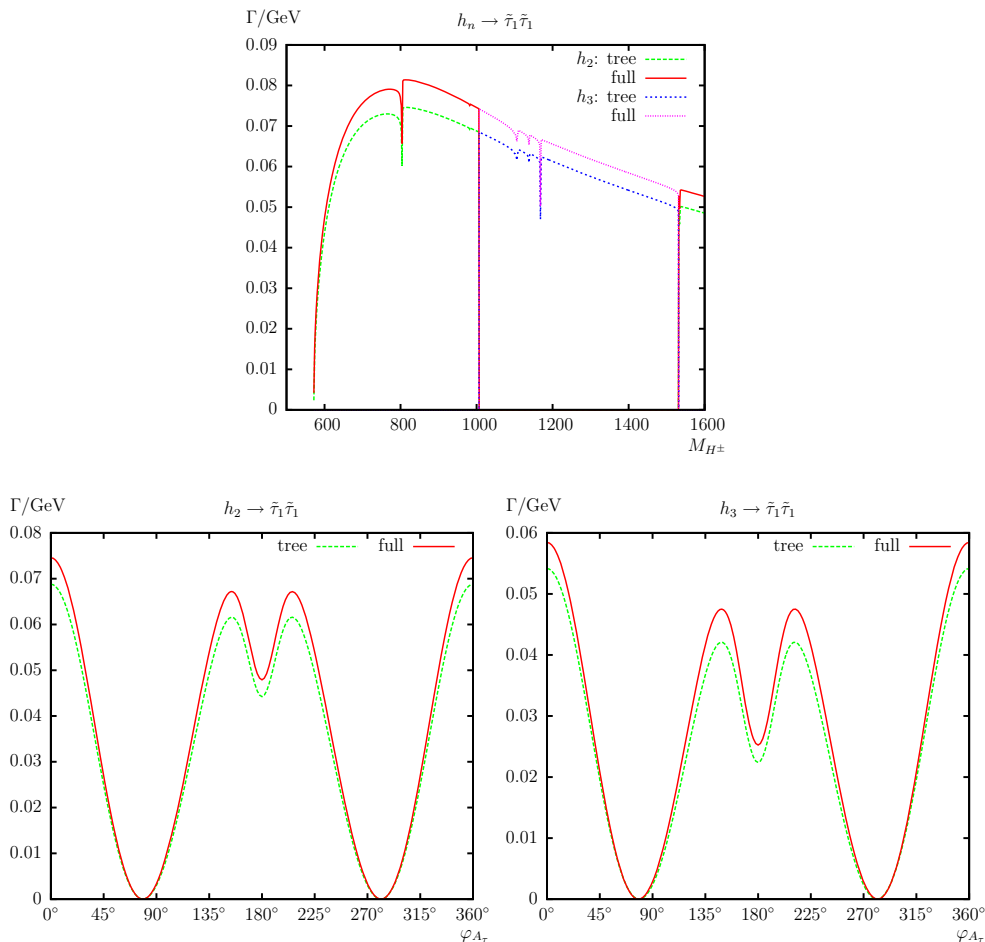
Fig. 17 $\Gamma(h_n \to \tilde{\tau}_1 \tilde{\tau}_1)$. Tree-level and full one-loop corrected partial decay widths are shown. The *upper plot* shows the partial decay width with $M_{H^\pm}$ varied; the *lower plots* show the complex phase φ_{A_τ} varied for h_2 decays (*left*, S1) and h_3 decays (*right*, S2)

corrections are found to be $\sim -48\,\%$ at $M_{H^\pm} = 1000$ GeV (i.e. S1). Correspondingly, the decay $h_3 \to \tilde{\nu}_\tau \tilde{\nu}_\tau$ for real parameters is non-zero only between MC1 and MC2. The dips are the thresholds TN10, TN13, and TN14. The full relative corrections are $\sim -17\,\%$ at $M_{H^\pm} = 1400$ GeV (i.e. S2).

The dependence on φ_{A_τ} is shown for the h_2 (h_3) decay in the lower left (right) plot of Fig. 16 for $M_{H^\pm} = 1000$ (1400) GeV. The tree decay width is independent from φ_{A_τ} due to the absence of A_τ in the corresponding couplings $C(h_n, \tilde{\nu}_\tau, \tilde{\nu}_\tau)$, see Ref. [87], which can be clearly observed in both lower plots. For the h_2 decay the loop corrections can reach $\sim -40\,\%$ at $\varphi_{A_\tau} = 180°$. For the h_3 decay they can reach $\sim -12\,\%$ at $\varphi_{A_\tau} = 180°$.

In Fig. 17 we present the results for the decays $h_n \to \tilde{\tau}_1 \tilde{\tau}_1$. The upper row shows the decay widths as a function of $M_{H^\pm}$. As before, the decay width of h_2 is non-zero for real parameters only below MC1 and above MC2, whereas the h_3 decay width is non-zero between the two mass crossing points. Starting with h_2, the dips/thresholds are TN5 and TN8. The full relative corrections are $\sim +8\,\%$ at $M_{H^\pm} = 1000$ GeV (i.e. S1). The dips of the h_3 decay are (again) the thresh-

olds TN10, TN13 and TN14. The full relative corrections at $M_{H^\pm} = 1400$ GeV (i.e. S2) are $\sim +8\,\%$.

In the lower left plot of Fig. 17 we show the h_2 decay with φ_{A_τ} varied at $M_{H^\pm} = 1000$ GeV. Here the loop corrections can reach $\sim +9\,\%$ around $\varphi_{A_\tau} \sim 140°$, $220°$. For S1 we have $h_2 \sim H$ and the $\hat{\mathbf{Z}}$ matrix depends rather weak on A_τ, i.e. the main effect on the decay width stems *continuously* from the $\hat{\mathbf{Z}}$ matrix element $\hat{Z}_{22}$. The tree decay width goes to zero at $\varphi_{A_b} \approx 78°$, $282°$, because the relevant ($\propto \hat{Z}_{22}$) real part of the coupling $C(h_2, \tilde{\tau}_1, \tilde{\tau}_1)$, see Ref. [87], accidentally goes through zero. In the lower right plot of Fig. 17 we show h_3 results as a function of φ_{A_τ} with $M_{H^\pm} = 1400$ GeV. Here the loop corrections can reach $\sim +13\,\%$ at $\varphi_{A_\tau} \sim 140°$, $220°$, and we have $h_2 \sim H$ in S2, which leads to a vanishing width around $\varphi_{A_\tau} \sim 78°$, $282°$. Here, this is again because the relevant ($\propto \hat{Z}_{32}$) real part of the coupling $C(h_3, \tilde{\tau}_1, \tilde{\tau}_1)$ accidentally goes through zero.

Finally, in Fig. 18 we present the results for $\Gamma(h_n \to \tilde{\tau}_2 \tilde{\tau}_2)$, which are shown in full analogy to $\Gamma(h_n \to \tilde{\tau}_1 \tilde{\tau}_1)$ above. As before, for real parameters, the h_2 decay width is found non-zero only below MC1 and above MC2, while the
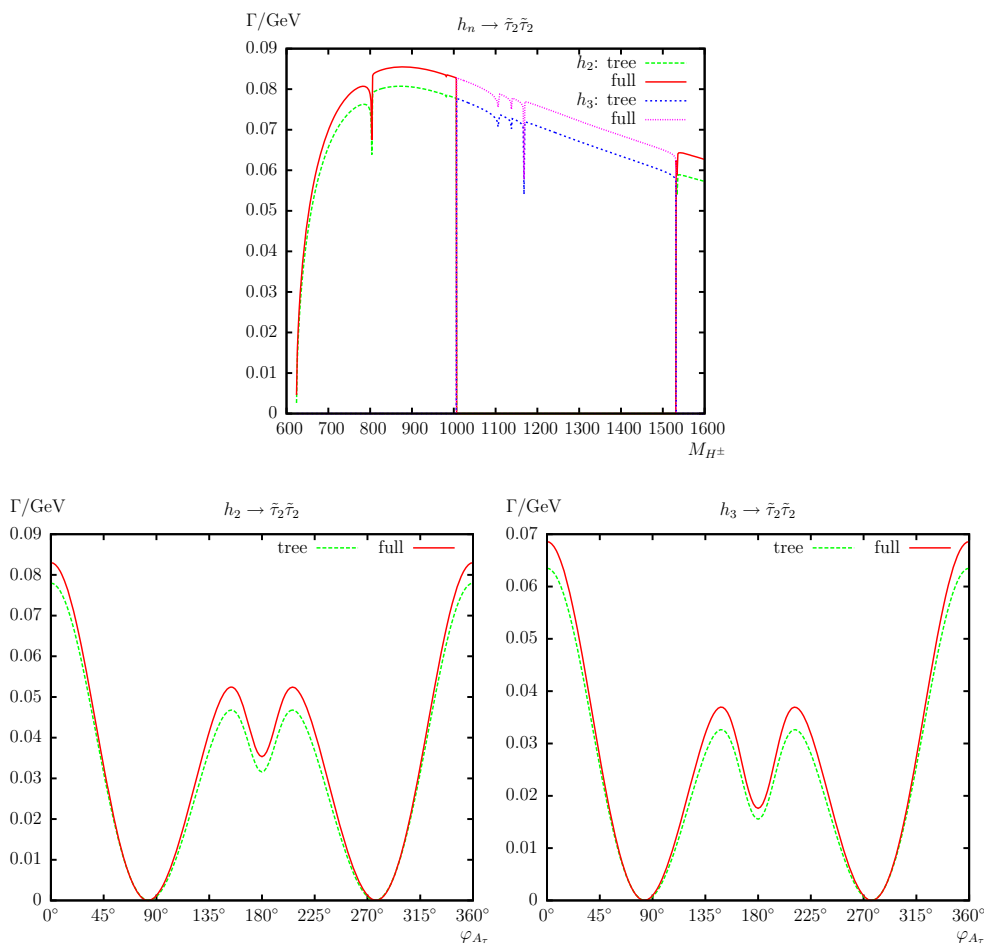
Fig. 18 $\Gamma(h_n \to \tilde{\tau}_2 \tilde{\tau}_2)$. Tree-level and full one-loop corrected partial decay widths are shown. The *upper plot* shows the partial decay width with $M_{H^\pm}$ varied; the *lower plots* show the complex phase φ_{A_τ} varied for h_2 decays (*left*, S1) and h_3 decays (*right*, S2)

h_3 width is non-zero only between MC1 and MC2. The h_n decay widths as a function of $M_{H^\pm}$ exhibit the same dips as in Fig. 17; see above. The full relative corrections to the h_2 width are $\sim$+6 % at $M_{H^\pm} = 1000$ GeV (i.e. S1). The full relative corrections to the h_3 decay at $M_{H^\pm} = 1400$ GeV (i.e. S2) are $\sim$+8 %.

In the lower left plot of Fig. 18 we show the h_2 decay with φ_{A_τ} varied at $M_{H^\pm} = 1000$ GeV. Here the loop corrections can reach $\sim$+12 % at $\varphi_{A_\tau} \sim 140°$, 180°, 220°. The decay width goes to zero in analogy to Fig. 17. In the right plot of Fig. 18 the corresponding h_3 results are shown for $M_{H^\pm} = 1400$ GeV, where we find the same level of higher-order corrections, and the dominating effect of the $\hat{\mathbf{Z}}$ matrix (in combination with the $C(h_{2,3}, \tilde{\tau}_2, \tilde{\tau}_2)$ couplings) as in Fig. 17.

5 Conclusions

We evaluated all partial decay widths corresponding to a two-body decay of the heavy MSSM Higgs bosons to scalar fermions, allowing for complex parameters. The decay modes are given in Eqs. (1) and (2). The evaluation is based on a full one-loop calculation of all decay channels, also including hard QED and QCD radiation. In the case of a discovery of additional Higgs bosons a subsequent precision measurement of their properties will be crucial to determine their nature and the underlying (SUSY) parameters. In order to yield a sufficient accuracy, one-loop corrections to the various Higgs-boson decay modes have to be considered. With the full one-loop calculation here presented for scalar fermions another step in the direction of a complete one-loop evaluation of all possible decay modes has been taken.

We first reviewed the one-loop renormalization procedure of the cMSSM, which is relevant for our calculation. In most cases we follow Ref. [57]. However, in the scalar sfermion sector, where we differ from Ref. [57] all relevant details are given.

We have discussed the calculation of the one-loop diagrams, the treatment of UV and IR divergences that are canceled by the inclusion of (hard and soft) QCD and QED radiation. We have checked our result against the literature (where loop corrections so far only for real parameters were

Table 4 Thresholds in neutral Higgs-boson decays

TN1:	$M_{H^\pm} \approx$ 598 GeV	$m_{\tilde{\chi}_1^0} + m_{\tilde{\chi}_1^0} = m_{h_2} \approx$ 591 GeV
TN2:	$M_{H^\pm} \approx$ 624 GeV	$m_{\tilde{\tau}_2} + m_{\tilde{\tau}_2} = m_{h_2} =$ 618 GeV
TN3:	$M_{H^\pm} \approx$ 775 GeV	$m_{\tilde{\chi}_1^0} + m_{\tilde{\chi}_2^0} = m_{h_3} \approx$ 771 GeV
TN4:	$M_{H^\pm} \approx$ 794 GeV	$m_{\tilde{\tau}_1} + m_{\tilde{\tau}_1} = m_{h_2} =$ 788 GeV
TN5:	$M_{H^\pm} \approx$ 805 GeV	$m_{\tilde{\chi}_1^0} + m_{\tilde{\chi}_3^0} = m_{h_2} \approx$ 799 GeV
TN6:	$M_{H^\pm} \approx$ 948 GeV	$m_{\tilde{\chi}_1^\pm} + m_{\tilde{\chi}_1^\pm} = m_{h_3} \approx$ 945 GeV
TN7:	$M_{H^\pm} \approx$ 954 GeV	$m_{\tilde{\chi}_2^0} + m_{\tilde{\chi}_2^0} = m_{h_3} \approx$ 951 GeV
TN8:	$M_{H^\pm} \approx$ 982 GeV	$m_{\tilde{\chi}_2^0} + m_{\tilde{\chi}_3^0} = m_{h_2} \approx$ 979 GeV
TN9:	$M_{H^\pm} \approx$ 1092 GeV	$m_{\tilde{b}_1} + m_{\tilde{b}_2} = m_{h_2} \approx$ 1086 GeV
TN10:	$M_{H^\pm} \approx$ 1107 GeV	$m_{\tilde{\chi}_1^\pm} + m_{\tilde{\chi}_2^\pm} = m_{h_3} \approx$ 1105 GeV
TN11:	$M_{H^\pm} \approx$ 1108 GeV	$m_{\tilde{\chi}_1^\pm} + m_{\tilde{\chi}_2^\pm} = m_{h_2} \approx$ 1105 GeV
TN12:	$M_{H^\pm} \approx$ 1112 GeV	$m_{\tilde{\chi}_2^0} + m_{\tilde{\chi}_4^0} = m_{h_2} \approx$ 1108 GeV
TN13:	$M_{H^\pm} \approx$ 1138 GeV	$m_{\tilde{\chi}_3^0} + m_{\tilde{\chi}_4^0} = m_{h_3} \approx$ 1135 GeV
TN14:	$M_{H^\pm} \approx$ 1168 GeV	$m_{\tilde{\tau}_1} + m_{\tilde{\tau}_2} = m_{h_3} =$ 1165 GeV
TN15:	$M_{H^\pm} \approx$ 1171 GeV	$m_{\tilde{\tau}_1} + m_{\tilde{\tau}_2} = m_{h_2} =$ 1165 GeV
TN16:	$M_{H^\pm} \approx$ 1268 GeV	$m_{\tilde{\chi}_2^\pm} + m_{\tilde{\chi}_2^\pm} = m_{h_2} \approx$ 1264 GeV
TN17:	$M_{H^\pm} \approx$ 1268 GeV	$m_{\tilde{\chi}_4^0} + m_{\tilde{\chi}_4^0} = m_{h_2} \approx$ 1265 GeV
TN18:	$M_{H^\pm} \approx$ 1545 GeV	$m_{\tilde{\tau}_2} + m_{\tilde{\tau}_2} = m_{h_2} =$ 1542 GeV

available) and in most cases found good agreement, once our set-up was changed to the one used in the existing analyses.

While the analytical calculation has been performed for *all* decay modes to sfermions, in the numerical analysis we concentrated on the decays to the third generation sfermions: scalar tops, bottoms, taus, and tau neutrinos. For the analysis we have chosen a parameter set that allows simultaneously a maximum number of two-body sfermionic decay modes. In the analysis either the charged Higgs-boson mass or the phase of a relevant trilinear coupling has been varied. For $M_{H^\pm}$ we investigated an interval starting at $M_{H^\pm} = 600$ GeV up to $M_{H^\pm} = 1.6$ TeV, which roughly coincides with the reach of the LHC for high-luminosity running as well as an e^+e^- collider with a center-of-mass energy up to $\sqrt{s} \sim 3$ TeV.

In our numerical scenarios we compared the tree-level partial decay widths with the full one-loop corrected partial decay widths. In the case of decays to scalar quarks we also included for comparison the pure SQCD one-loop corrections. We concentrated on the analysis of the decay widths themselves, since the size of the corresponding branching ratios (and thus the size of the one-loop effects) is highly parameter dependent.

We found sizable, roughly $\mathcal{O}(15\,\%)$, corrections in all the channels. The corrections tend to be larger for the decays to scalar quarks w.r.t. decays to scalar leptons. For some parts of the parameter space (not only close to thresholds) also larger corrections up to 30 or 40 % (and in exceptional cases even higher) have been observed. Consequently, the full one-loop corrections should be taken into account for the interpretation

of the searches for scalar fermions as well as for any future precision analyses of those decays.

The size of the tree-level decay widths and of the corresponding full one-loop corrections often depend strongly on the respective complex phase, i.e. φ_{A_t}, φ_{A_b} or φ_{A_τ}. The one-loop contributions often vary by a factor of $2-3$ as a function of the complex phases and sometimes can even turn negative. Neglecting the phase dependence could lead to a wrong impression of the relative size of the various decay widths. Furthermore, for certain values of the phases the relevant ($\propto \hat{\mathbf{Z}}$ matrix) real parts of specific couplings accidentally go through zero. Consequently, also the decay widths go to zero for these values, where the $\hat{\mathbf{Z}}$ matrix yields the dominating effect on the widths.

In case of decays to scalar quarks we have also compared with the pure SQCD result. We have found that in most cases the EW corrections are of similar size. Neglecting those can lead, depending on the parameter space, to a large over- or underestimate of the full one-loop corrections.

In the cases where a decay and its complex conjugate final state are possible we have evaluated both decay widths independently. The asymmetries, as a byproduct of our calculation, turn out to be sizable, in particular for decays into a pair of lighter and heavier scalar fermions.

The numerical results we have shown are, of course, dependent on the choice of the SUSY parameters. Nevertheless, they give an idea of the relevance of the full one-loop corrections. Decay channels (and their respective one-loop corrections) that may look unobservable due to the smallness of their decay width in our numerical examples could become important if other channels are kinematically forbidden. Following our analysis it is evident that the full one-loop corrections are mandatory for a precise prediction of the various branching ratios. We emphasize again that in many cases it is not sufficient to include only SQCD corrections, as electroweak corrections can be of comparable size. The full one-loop corrections should be taken into account in any precise determination of (SUSY) parameters from the decay of heavy MSSM Higgs bosons. The results for the heavy MSSM Higgs-boson decays will be implemented into the Fortran code FeynHiggs.

References

1. H. Nilles, Phys. Rep. **110**, 1 (1984)
2. R. Barbieri, Riv. Nuovo Cim. **11**, 1 (1988)
3. H. Haber, G. Kane, Phys. Rep. **117**, 75 (1985)
4. J. Gunion, H. Haber, Nucl. Phys. B **272**, 1 (1986)
5. G. Aad et al. (ATLAS Collaboration), Phys. Lett. B **716**, 1 (2012). arXiv:1207.7214 [hep-ex]
6. S. Chatrchyan et al. (CMS Collaboration), Phys. Lett. B **716**, 30 (2012). arXiv:1207.7235 [hep-ex]
7. G. Aad et al. (ATLAS Collaboration), JHEP **1411**, 056 (2014). arXiv:1409.6064 [hep-ex]
8. V. Khachatryan et al. (CMS Collaboration), JHEP **1410**, 160 (2014). arXiv:1408.3316 [hep-ex]
9. A. Holzner (ATLAS and CMS Collaborations), arXiv:1411.0322 [hep-ex]
10. H. Baer et al., The international linear collider technical design report—volume 2: Physics, arXiv:1306.6352 [hep-ph]
11. TESLA Technical Design Report (TESLA Collaboration) Part 3, Physics at an e^+e^- linear collider. arXiv:hep-ph/0106315. See http://www.tesla.desy.de/new_pages/TDR_CD/start.html
12. K. Ackermann et al., DESY-PROC-2004-01
13. J. Brau et al. (ILC Collaboration), ILC reference design report volume 1—executive summary. arXiv:0712.1950 [physics.acc-ph]
14. G. Aarons et al. (ILC Collaboration), International linear collider reference design report volume 2: physics at the ILC. arXiv:0709.1893 [hep-ph]
15. L. Linssen, A. Miyamoto, M. Stanitzki, H. Weerts, arXiv:1202.5940 [physics.ins-det]
16. H. Abramowicz et al. (CLIC Detector and Physics Study Collaboration), Physics at the CLIC e^+e^- linear collider—input to the snowmass process 2013. arXiv:1307.5288 [hep-ex]
17. G. Weiglein et al. (LHC/ILC Study Group), Phys. Rep. **426**, 47 (2006). arXiv:hep-ph/0410364
18. A. De Roeck et al., Eur. Phys. J. C **66**, 525 (2010). arXiv:0909.3240 [hep-ph]
19. A. De Roeck, J. Ellis, S. Heinemeyer, CERN Cour. **49N10**, 27 (2009)
20. K. Williams, H. Rzehak, G. Weiglein, Eur. Phys. J. C **71**, 1669 (2011). arXiv:1103.1335 [hep-ph]
21. S. Heinemeyer, W. Hollik, G. Weiglein, Eur. Phys. J. C **16**, 139 (2000). arXiv:hep-ph/0003022
22. D. Noth, M. Spira, Phys. Rev. Lett. **101**, 181801 (2008). arXiv:0808.0087 [hep-ph]
23. D. Noth, M. Spira, JHEP **1106**, 084 (2011). arXiv:1001.1935 [hep-ph]
24. L. Mihaila, C. Reisser, JHEP **1008**, 021 (2010). arXiv:1007.0693 [hep-ph]
25. R. Hempfling, Phys. Rev. D **49**, 6168 (1994)
26. L. Hall, R. Rattazzi, U. Sarid, Phys. Rev. D **50**, 7048 (1994). arXiv:hep-ph/9306309
27. M. Carena, M. Olechowski, S. Pokorski, C. Wagner, Nucl. Phys. B **426**, 269 (1994). arXiv:hep-ph/9402253
28. M. Carena, D. Garcia, U. Nierste, C. Wagner, Nucl. Phys. B **577**, 577 (2000). arXiv:hep-ph/9912516
29. S. Heinemeyer, W. Hollik, Nucl. Phys. B **474**, 32 (1996). arXiv:hep-ph/9602318
30. A. Bredenstein, A. Denner, S. Dittmaier, M. Weber, Phys. Rev. D **74**, 013004 (2006). arXiv:hep-ph/0604011
31. A. Bredenstein, A. Denner, S. Dittmaier, M. Weber, JHEP **0702**, 080 (2007). arXiv:hep-ph/0611234
32. A. Bredenstein, A. Denner, S. Dittmaier, A. Mück, M. Weber, see http://omnibus.uni-freiburg.de/~sd565/programs/prophecy4f/prophecy4f.html
33. M. Frank, T. Hahn, S. Heinemeyer, W. Hollik, H. Rzehak, G. Weiglein, JHEP **0702**, 047 (2007). arXiv:hep-ph/0611326
34. S. Heinemeyer, W. Hollik, G. Weiglein, Eur. Phys. J. C **9**, 343 (1999). arXiv:hep-ph/9812472
35. S. Heinemeyer, W. Hollik, G. Weiglein, Comput. Phys. Commun. **124**, 76 (2000). arXiv:hep-ph/9812320
36. T. Hahn, S. Heinemeyer, W. Hollik, H. Rzehak, G. Weiglein, Comput. Phys. Commun. **180**, 1426 (2009). See www.feynhiggs.de
37. G. Degrassi, S. Heinemeyer, W. Hollik, P. Slavich, G. Weiglein, Eur. Phys. J. C **28**, 133 (2003). arXiv:hep-ph/0212020
38. T. Hahn, S. Heinemeyer, W. Hollik, H. Rzehak, G. Weiglein, Phys. Rev. Lett. **112**, 141801 (2014). arXiv:1312.4937 [hep-ph]
39. A. Djouadi, J. Kalinowsli, M. Spira, Comput. Phys. Commun. **108**, 56 (1998). arXiv:hep-ph/9704448
40. M. Spira, Fortschr. Phys. **46**, 203 (1998). arXiv:hep-ph/9705337
41. A. Djouadi, J. Kalinowski, M. Mühlleitner, M. Spira, arXiv:1003.1643 [hep-ph]
42. S. Heinemeyer et al. (LHC Higgs Cross Section Working Group), arXiv:1307.1347 [hep-ph]
43. M. Carena, S. Heinemeyer, O. Stål, C. Wagner, G. Weiglein, Eur. Phys. J. C **73**, 2552 (2013). arXiv:1302.7033 [hep-ph]
44. A. Bartl, H. Eberl, K. Hidaka, T. Kon, W. Majerotto, Y. Yamada, Phys. Lett. B **373**, 117 (1996). arXiv:hep-ph/9508283
45. A. Bartl, H. Eberl, K. Hidaka, T. Kon, W. Majerotto, Y. Yamada, Phys. Lett. B **402**, 303 (1997). arXiv:hep-ph/9701398
46. H. Eberl, K. Hidaka, S. Kraml, W. Majerotto, Y. Yamada, Phys. Rev. D **62**, 055006 (2000). arXiv:hep-ph/9912463
47. C. Weber, H. Eberl, W. Majerotto, Phys. Lett. B **572**, 56 (2003). arXiv:hep-ph/0305250
48. C. Weber, H. Eberl, W. Majerotto, Phys. Rev. D **68**, 093011 (2003). arXiv:hep-ph/0308146
49. C. Weber, K. Kovarik, H. Eberl, W. Majerotto, Nucl. Phys. B **776**, 138 (2007). arXiv:hep-ph/0701134
50. W. Frisch, H. Eberl, H. Hluchá, Comput. Phys. Commun. **182**, 2219 (2011). arXiv:1012.5025 [hep-ph]
51. S. Heinemeyer, H. Rzehak, C. Schappacher, Phys. Rev. D **82**, 075010 (2010). arXiv:1007.0689 [hep-ph]
52. S. Heinemeyer, H. Rzehak, C. Schappacher, PoSCHARGED **2010**, 039 (2010). arXiv:1012.4572 [hep-ph]
53. T. Fritzsche, S. Heinemeyer, H. Rzehak, C. Schappacher, Phys. Rev. D **86**, 035014 (2012). arXiv:1111.7289 [hep-ph]
54. S. Heinemeyer, C. Schappacher, Eur. Phys. J. C **72**, 2136 (2012). arXiv:1204.4001 [hep-ph]
55. A. Arhrib, A. Djouadi, W. Hollik, C. Jünger, Phys. Rev. D **57**, 5860 (1998). arXiv:hep-ph/9702426
56. E. Accomando, G. Chachamis, F. Fugel, M. Spira, M. Walser, Phys. Rev. D **85**, 015004 (2012). arXiv:1103.4283 [hep-ph]
57. T. Fritzsche, T. Hahn, S. Heinemeyer, F. von der Pahlen, H. Rzehak, C. Schappacher, Comput. Phys. Commun. **185**, 1529 (2014). arXiv:1309.1692 [hep-ph]
58. S. Heinemeyer, W. Hollik, H. Rzehak, G. Weiglein, Phys. Lett. B **652**, 300 (2007). arXiv:0705.0746 [hep-ph]
59. H. Rzehak, PhD thesis: Two-loop contributions in the supersymmetric Higgs sector. Technische Universität München, 2005. See http://www.nbn-resolving.de/ with URN: nbn:de:bvb:91-diss20050923-0853568146
60. A. Bartl, H. Eberl, K. Hidaka, S. Kraml, W. Majerotto, W. Porod, Y. Yamada, Phys. Lett. B **419**, 243 (1998). arXiv:hep-ph/9710286
61. A. Bartl, H. Eberl, K. Hidaka, S. Kraml, W. Majerotto, W. Porod, Y. Yamada, Phys. Rev. D **59**, 115007 (1999). arXiv:hep-ph/9806299
62. A. Djouadi, P. Gambino, S. Heinemeyer, W. Hollik, C. Jünger, G. Weiglein, Phys. Rev. Lett. **78**, 3626 (1997). arXiv:hep-ph/9612363

63. A. Djouadi, P. Gambino, S. Heinemeyer, W. Hollik, C. Jünger, G. Weiglein, Phys. Rev. D **57**, 4179 (1998). arXiv:hep-ph/9710438
64. W. Hollik, H. Rzehak, Eur. Phys. J. C **32**, 127 (2003). arXiv:hep-ph/0305328
65. S. Heinemeyer, W. Hollik, H. Rzehak, G. Weiglein, Eur. Phys. J. C **39**, 465 (2005). arXiv:hep-ph/0411114
66. J. Beringer et al. (Particle Data Group), Phys. Rev. D **86** (2012) 010001 and 2013 partial update for the 2014 edition
67. K. Chetyrkin, J. Kühn, M. Steinhauser, Comput. Phys. Commun. **133**, 43 (2000). arXiv:hep-ph/0004189
68. B. Schmidt, M. Steinhauser, Comput. Phys. Commun. **183**, 1845 (2012). arXiv:1201.6149 [hep-ph]
69. M. Carena, D. Garcia, U. Nierste, C. Wagner, Nucl. Phys. B **577**, 577 (2000). arXiv:hep-ph/9912516
70. L. Hall, R. Rattazzi, U. Sarid, Phys. Rev. D **50**, 7048 (1994). arXiv:hep-ph/9306309
71. M. Carena, M. Olechowski, S. Pokorski, C. Wagner, Nucl. Phys. B **426**, 269 (1994). arXiv:hep-ph/9402253
72. M. Carena, J. Ellis, A. Pilaftsis, C. Wagner, Nucl. Phys. B **586**, 92 (2000). arXiv:hep-ph/0003180
73. J. Guasch, P. Hafliger, M. Spira, Phys. Rev. D **68**, 16 (2003). arXiv:hep-ph/0305101
74. R. Harlander, L. Mihaila, M. Steinhauser, Phys. Rev. D **72**, 095009 (2005). arXiv:hep-ph/0509048
75. R. Harlander, L. Mihaila, M. Steinhauser, Phys. Rev. D **76**, 055002 (2007). arXiv:0706.2953 [hep-ph]
76. A. Denner, S. Dittmaier, M. Roth, D. Wackeroth, Nucl. Phys. B **560**, 33 (1999). arXiv:hep-ph/9904472
77. J. Küblbeck, M. Böhm, A. Denner, Comput. Phys. Commun. **60**, 165 (1990)
78. T. Hahn, Comput. Phys. Commun. **140**, 418 (2001). arXiv:hep-ph/0012260
79. T. Hahn, C. Schappacher, Comput. Phys. Commun. **143**, 54 (2002). hep-ph/0105349. Program, user's guide and model files are available via www.feynarts.de
80. T. Hahn, M. Pérez-Victoria, Comput. Phys. Commun. **118**, 153 (1999). arXiv:hep-ph/9807565
81. F. del Aguila, A. Culatti, R. Muñoz Tapia, M. Pérez-Victoria, Nucl. Phys. B **537**, 561 (1999). arXiv:hep-ph/9806451
82. W. Siegel, Phys. Lett. B **84**, 193 (1979)
83. D. Capper, D. Jones, P. van Nieuwenhuizen, Nucl. Phys. B **167**, 479 (1980)
84. D. Stöckinger, JHEP **0503**, 076 (2005). arXiv:hep-ph/0503129
85. W. Hollik, D. Stöckinger, Phys. Lett. B **634**, 63 (2006). arXiv:hep-ph/0509298
86. A. Denner, Fortsch. Phys. **41**, 307 (1993). arXiv:0709.1075 [hep-ph]
87. The couplings can be found in HMix.ps.gz as part of the FeynArts package [58]
88. A. Arhrib, Private communication, 08.06.2014
89. J. Aguilar-Saavedra et al., Eur. Phys. J. C **46**, 43 (2006). arXiv:hep-ph/0511344
90. J. Frère, D. Jones, S. Raby, Nucl. Phys. B **222**, 11 (1983)
91. M. Claudson, L. Hall, I. Hinchliffe, Nucl. Phys. B **228**, 501 (1983)
92. C. Kounnas, A. Lahanas, D. Nanopoulos, M. Quiros, Nucl. Phys. B **236**, 438 (1984)
93. J. Gunion, H. Haber, M. Sher, Nucl. Phys. B **306**, 1 (1988)
94. J. Casas, A. Lleyda, C. Munoz, Nucl. Phys. B **471**, 3 (1996). arXiv:hep-ph/9507294
95. P. Langacker, N. Polonsky, Phys. Rev. D **50**, 2199 (1994). arXiv:hep-ph/9403306
96. A. Strumia, Nucl. Phys. B **482**, 24 (1996). arXiv:hep-ph/9604417
97. S. Dimopoulos, S. Thomas, Nucl. Phys. B **465**, 23 (1996). arXiv:hep-ph/9510220
98. M. Dugan, B. Grinstein, L. Hall, Nucl. Phys. B **255**, 413 (1985)
99. D. Demir, O. Lebedev, K. Olive, M. Pospelov, A. Ritz, Nucl. Phys. B **680**, 339 (2004). arXiv:hep-ph/0311314
100. D. Chang, W. Keung, A. Pilaftsis, Phys. Rev. Lett. **82**, 900 (1999). hep-ph/9811202 [Erratum-ibid. **83**, 3972 (1999)]
101. A. Pilaftsis, Phys. Lett. B **471**, 174 (1999). arXiv:hep-ph/9909485
102. O. Lebedev, K. Olive, M. Pospelov, A. Ritz, Phys. Rev. D **70**, 016003 (2004). arXiv:hep-ph/0402023
103. W. Hollik, J. Illana, S. Rigolin, D. Stöckinger, Phys. Lett. B **416**, 345 (1998). arXiv:hep-ph/9707437
104. W. Hollik, J. Illana, S. Rigolin, D. Stöckinger, Phys. Lett. B **425**, 322 (1998). arXiv:hep-ph/9711322
105. P. Nath, Phys. Rev. Lett. **66**, 2565 (1991)
106. Y. Kizukuri, N. Oshimo, Phys. Rev. D **46**, 3025 (1992)
107. T. Ibrahim, P. Nath, Phys. Lett. B **418**, 98 (1998). arXiv:hep-ph/9707409
108. T. Ibrahim, P. Nath, Phys. Rev. D **57**, 478 (1998). arXiv:hep-ph/9708456 [Erratum-ibid. D **58**, 019901 (1998); Erratum-ibid. D **60**, 079903 (1998); Erratum-ibid. D **60**, 119901 (1999)]
109. M. Brhlik, G. Good, G. Kane, Phys. Rev. D **59**, 115004 (1999). arXiv:hep-ph/9810457
110. S. Abel, S. Khalil, O. Lebedev, Nucl. Phys. B **606**, 151 (2001). arXiv:hep-ph/0103320
111. Y. Li, S. Profumo, M. Ramsey-Musolf, JHEP **1008**, 062 (2010). arXiv:1006.1440 [hep-ph]
112. V. Barger, T. Falk, T. Han, J. Jiang, T. Li, T. Plehn, Phys. Rev. D **64**, 056007 (2001). arXiv:hep-ph/0101106
113. H. Heath, C. Lynch, S. Moretti, C. Shepherd-Themistocleous, arXiv:0901.1676 [hep-ph]
114. A. Datta, A. Djouadi, M. Guchait, F. Moortgat, Nucl. Phys. B **681**, 31 (2004). arXiv:hep-ph/0303095
115. G. 't Hooft, M. Veltman, Nucl. Phys. B **153**, 365 (1979)